PhD Thesis

Experimental and theoretical study about drop impact on inclined surfaces and substrates with different roughness and wettability

Author: Paula García Geijo

Advisors: José Manuel Gordillo Arias de Saavedra

Guillaume Riboux Acher

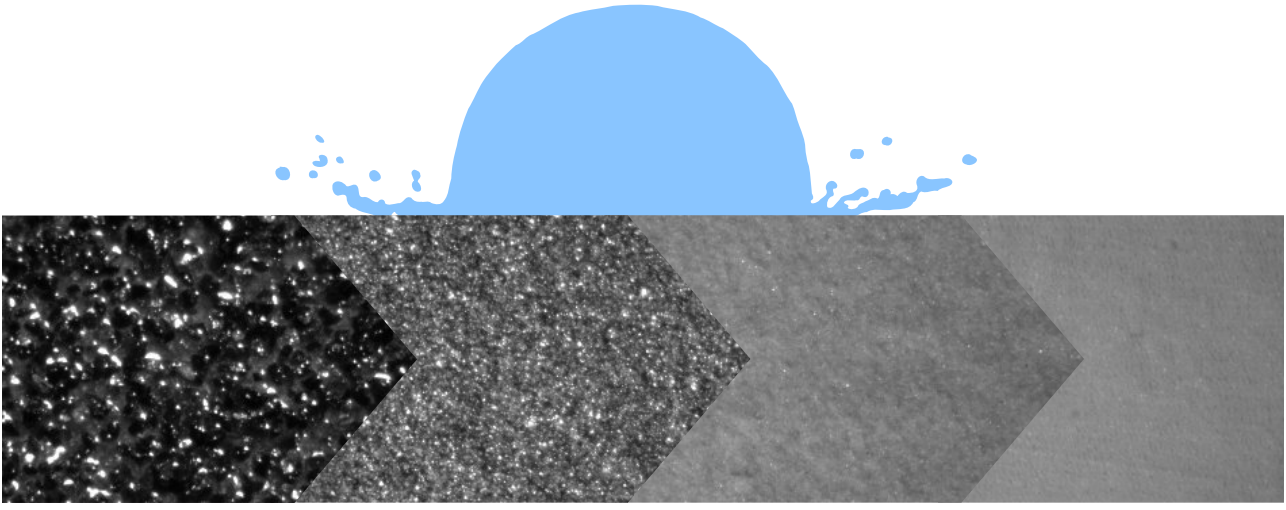

Sevilla, 2023

Tesis Doctoral

Experimental and theoretical study about drop impact on inclined surfaces and substrates with different roughness and wettability

Autor:

Paula García Geijo

Directores:

José Manuel Gordillo Arias de Saavedra

Catedrático

Guillaume Riboux

Profesor Titular

Departamento de Ingeniería Aeroespacial y Mecánica de Fluidos
Escuela Técnica Superior de Ingeniería
Universidad de Sevilla

2023

Tesis Doctoral: Experimental and theoretical study about drop impact on inclined surfaces and substrates with different roughness and wettability

Autor: Paula García Geijo
Directores: José Manuel Gordillo Arias de Saavedra
Guillaume Riboux

El tribunal nombrado para juzgar la Tesis arriba indicada, compuesto por los siguientes doctores:

Presidente:

Vocales:

Secretario:

acuerdan otorgarle la calificación de:

El Secretario del Tribunal

Fecha:

A mi familia,
fuente de apoyo y
amor incondicional

A Alber,
mi compañero

Agradecimientos

Finalizando esta tesis no se me pueden venir a la mente más que buenos recuerdos y eso es únicamente debido a la gente que me ha acompañado a lo largo de este camino. Tengo mucho que agradecer y tengo claro por donde empezar: mis directores de tesis.

José Manuel Gordillo y Guillaume Riboux son los principales culpables de que esta tesis y mi doctorado sean una realidad. Muchas gracias por confiar en mí y darme esta oportunidad, por todo lo que he aprendido con vosotros, de mecánica de fluidos y de la vida, pero sobre todo por lo bien que me habéis acogido y por hacerme sentir como en casa a pesar de no estar en mi querido León. Transmitís pasión por la ciencia y eso hace que sea un gusto trabajar con vosotros.

I also wanted to thank Detlef Lohse for giving me the opportunity to spend a few months at University of Twente. I really enjoyed my stay at Physics of Fluids group where I met a lot of people from the fluid mechanics community doing research in different topics. This experience has definitely helped me to broaden my knowledge, and in general, to broaden my mind. These four months in Enschede would have not been the same without the PoFDocs: Javi, Lorène, Vincent, Alex, Youssef, Udo, Ambre and Pierre. I miss our Monday pubquiz, home made dinners, playing cards and board games and having drinks at our base: Stanislaus.

Gracias también a mis amigos de Sevilla y a mis amigas de San Justo - Astorga. Ellos han sido la mejor compañía en la celebración de los buenos momentos, y también han hecho que los malos sean más llevaderos. Pero sin duda, el que más ha aguantado los míticos agobios de Paula, sobre todo estos últimos meses, es Alber. Muchas gracias por estar siempre a mi lado, apoyarme y sacar lo mejor de mí.

Por último, aunque para nada lo menos importante: mi familia. Gracias papá, mamá y Nuri. Aunque esta etapa la hayamos tenido que vivir desde la distancia, no me han faltado vuestro cariño y vuestros consejos. Espero que estéis orgullosos de vuestra hija y hermana, porque yo no puedo estar más feliz de la familia que me ha tocado y los valores que me

habéis transmitido. Aunque no esté allí, parte de mi corazón siempre se queda en León.

Gracias a todos vosotros soy doctora, pero aún más importante, una mejor persona.

Paula García Geijo

Sevilla, 2023

Resumen

En esta tesis se abordan tres aspectos relacionados con el impacto de gotas sobre superficies lisas y rugosas, tanto hidrofílicas como hidrófobas. El estudio del impacto de gotas sobre sustratos sólidos puede clasificarse en: i) el análisis de la expansión, conocida como *spreading*, y posterior retracción (en caso de que la hubiere), y ii) en la determinación de la velocidad crítica a partir de la cual la gota se disgrega en otras más pequeñas (fenómeno denominado *splashing*).

Así, tras una breve introducción de los fenómenos a analizar, el segundo capítulo de esta tesis se dedicará al estudio de la evolución temporal de la expansión de gotas de líquidos de baja viscosidad al impactar sobre superficies lisas e inclinadas, siendo este proceso totalmente semejante al impacto de una gota formando una trayectoria inclinada con respecto a un substrato sólido horizontal. En estas situaciones, el proceso de expansión desarrolla asimetrías que no habían sido cuantificadas hasta la fecha.

El tercer y cuarto capítulos están relacionados entre sí. En ellos se realiza un análisis exhaustivo del proceso de *splashing* en superficies rugosas, tanto hidrofílicas como hidrófobas, y se logra construir un diagrama que permite determinar la velocidad de transición al *splash* a presión atmosférica en función de las propiedades materiales del líquido, del ángulo de contacto estático, así como de la rugosidad relativa de la superficie. Por tanto, en esta tesis se proporciona una descripción completa de la transición al *splash* sobre superficies genéricas que posee un claro interés tecnológico.

Abstract

This thesis addresses three different topics related to drop impact on smooth and rough surfaces, not only in the hydrophilic case but also for hydrophobic substrates. The analysis of the drop impact over solid substrates can be classified in: i) drop spreading and subsequent retraction (if any), and ii) determination of the critical velocity at which the droplet disintegrates into smaller pieces, the so-called splashing process.

Thus, once the problem at hand is introduced, the second chapter of this thesis is devoted to the study of the temporal evolution of the drop expansion that takes place when drops of low viscosity liquids impact over smooth inclined surfaces, being this process comparable to the impact of a drop following an inclined trajectory with respect to a horizontal substrate. In these cases, the drop expansion shows some asymmetries that had not been quantified hitherto.

Chapters three and four are interrelated. Here, we conduct an exhaustive analysis of the splash transition over rough surfaces, both hydrophilic and hydrophobic, and we elaborate a diagram that allows determining the spreading-splashing transition at atmospheric conditions as a function of the liquid material properties, the static contact angle, and of the relative surface roughness. Therefore, this thesis provides a complete description of the splashing process over arbitrary substrates that possesses a clear technological interest.

Índice

1 Introducción

What we know is a drop, what we do not know is an ocean.

Isaac Newton

Algo que nos resulta tan familiar, tan común y cotidiano como el impacto de una gota sobre una superficie ha capturado la atención de numerosos investigadores a lo largo de la historia. Hace ya más de 500 años este fenómeno atrajo la atención de Leonardo da Vinci, quien ilustró en una de las páginas del conocido como Códice Leicester o Códice Hammer [1] las observaciones experimentales mostradas en la figura 1.1 [2]. Leonardo da Vinci comprobó que, tras hacer impactar una gota contra una superficie horizontal, terminan desarrollándose finos ligamentos de líquido que se encuentran distribuidos alrededor de todo el perímetro de la gota y que son eyectados radialmente hacia fuera de la zona de impacto.

Más adelante, en 1877, Worthington realizó un análisis detallado de la fenomenología tan variada que surge al impactar una gota contra una superficie horizontal. En su contribu-

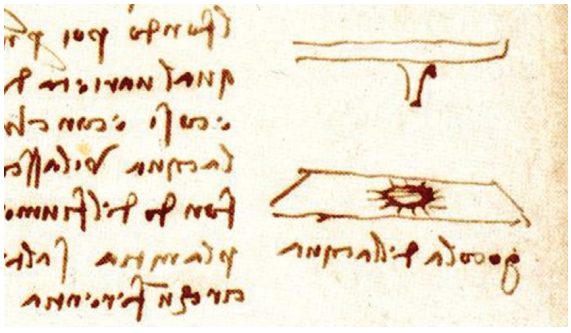

Figura 1.1 Esbozo de la marca que deja una gota de agua tras impactar en una sustrato horizontal realizado por Leonardo da Vinci en el margen del *folio 33r* del Códice Leicester [1]. Imagen tomada de la referencia [2].

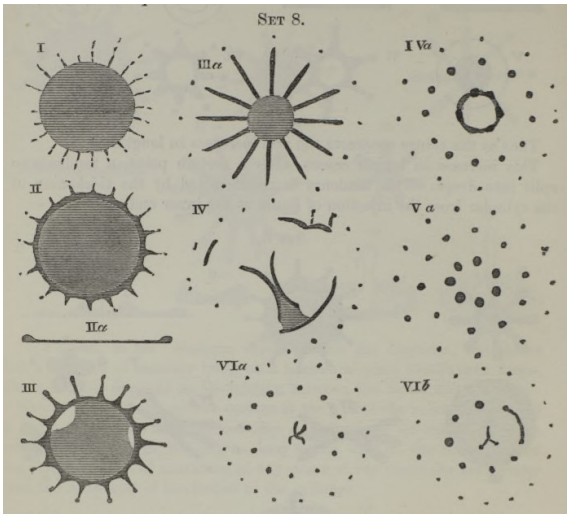

Figura 1.2 Ilustraciones de Worthington mostrando sus observaciones experimentales de *splash* al hacer impactar una gota de mercurio sobre una superficie horizontal. Se identifica la formación de los ligamentos distribuidos a lo largo de la gota desde los cuales se eyectan pequeñas gotas. A tiempos mayores (dibujos de la parte derecha) la gota se ha desintegrado completamente. Imagen tomada de la referencia [3].

ción, Worthington ilustra gráficamente los diferentes patrones que surgían al cambiar las propriedades materiales del líquido y el radio de la gota, así como la velocidad de impacto variando la altura de caída del líquido con respecto a la posición del sustrato [3, 4].

La dinámica del impacto de gotas sigue siendo de gran interés en la actualidad, y el motivo principal es que se trata de un fenómeno que está presente no solamente en multitud de situaciones cotidianas, sino también en diversas aplicaciones industriales: impresión con chorro de tinta, fenómenos de transferencia de calor donde es importante la cuantificación del área de contacto líquido-sólido, el estudio de la dispersión y propagación de enfermedades y productos contaminantes, e incluso también en los análisis forenses [5–10].

Como ya anticipó Worthington hace casi 150 años y como se ha ido descubriendo en estudios posteriores, el impacto de una gota sobre una superficie depende de una gran variedad de parámetros. No solo juegan un papel relevante la velocidad de impacto, las propiedades físicas del líquido y el radio de la gota, sino también otras propiedades como la rugosidad y mojabilidad de la superficie, su grado de inclinación, la presión atmosférica y las propiedades físicas del gas ambiente, así como el hecho de que el sustrato esté mojado o completamente seco, entre otros muchos.

Esta tesis se centra en el estudio del caso concreto del impacto de gotas milimétricas de líquidos de baja viscosidad a presión atmosférica sobre superficies secas e impermeables a una velocidad de impacto tal que los efectos inerciales dominan sobre los esfuerzos viscosos y las fuerzas de tensión superficial.

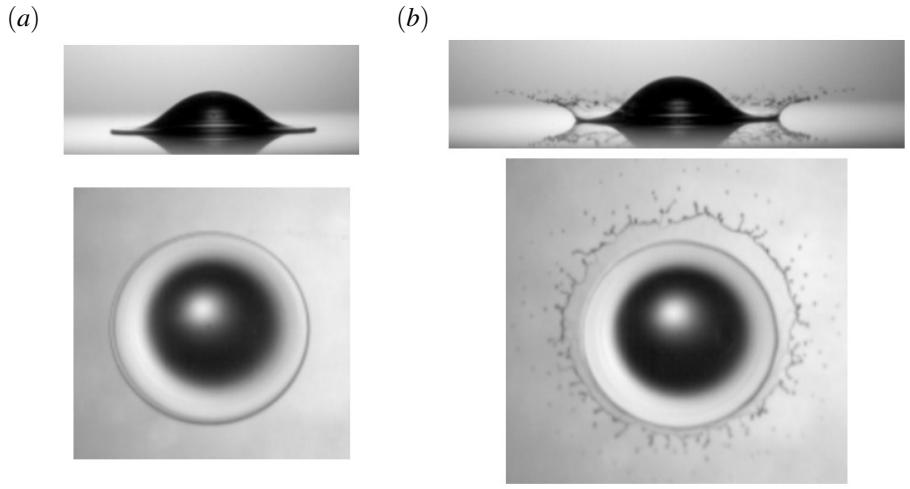

Figura 1.3 Vista lateral y cenital de los fenómenos de (*a*) *spreading* y (*b*) *splashing* producidos cuando una gota etanol impacta contra una placa de vidrio horizontal a una velocidad (a) inferior y (b) superior a la velocidad de transición al *splash*. Imágenes grabadas durante el estudio experimental realizado en esta tesis.

Los parámetros que se variarán y, por tanto, las características cuya influencia se analizará, serán la viscosidad del líquido, el tamaño de las rugosidades de la superficie, el ángulo de contacto que forma la gota con el sólido, que está relacionado con el grado de repelencia al agua del sustrato, y el ángulo de inclinación que forma la trayectoria que sigue la gota en el momento del impacto con la pared.

1.1 Definiciones previas

Durante los primeros instantes de tiempo tras el impacto de una gota contra una superficie, se pueden producir dos situaciones diferentes. Cuando la velocidad de impacto es baja, la gota se expande suavemente de forma tangencial al sustrato, dando lugar a lo que en la comunidad científica y en la literatura inglesa se conoce como *spreading* (ver figura 1.3a). Sin embargo, si la misma gota impacta a velocidades cada vez mayores, se observa que existe una velocidad crítica a partir de la cual la gota pierde su integridad, rompiéndose en pequeños fragmentos que son eyectados radialmente hacia fuera a velocidades mayores que la de impacto, fenómeno que se conoce comunmente como *splash* (ver figura 1.3b) [8, 11].

Respecto al fenómeno de desintegración de la gota, algunas contribuciones diferencian entre dos tipos de *splash* a la hora de analizar el proceso de rotura. Si se eyectan pocas gotas y de forma aproximadamente tangente a la superficie, el proceso se denomina *splash* puntual o *prompt splash*, mientras que se emplea el término *corona splash* para caracterizar aquellas situaciones en las que la lámina de líquido se separa de manera ostensible del sustrato y el número de gotas eyectadas es mucho mayor [12–15]. Sin embargo, en esta tesis no se atenderá a dicha distinción y el análisis se simplificará considerando que la

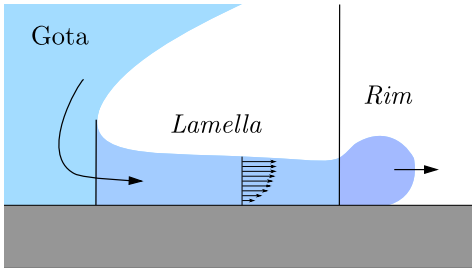

Figura 1.4 Esquema de las distintas regiones en las que se divide la gota para el estudio del proceso de expansión.

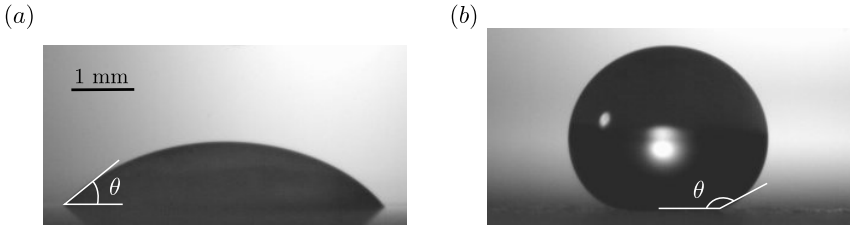

Figura 1.5 Imagen experimental de una gota de agua depositada sobre una superficie (a) hidrofílica, (b) hidrófoba. Se comprueba que el ángulo de contacto que forma el líquido con el sólido, que está relacionado con el grado de repelencia al agua, es menor que $\pi/2$ para las superficies hidrofílicas y mayor que $\pi/2$ para el caso de sustratos hidrófobos.

transición de *spreading* a *splashing* tiene lugar cuando la gota pierde su integridad y se rompe en gotas más pequeñas y rápidas, que son eyectadas con una velocidad mayor a la de impacto.

Durante el proceso de expansión, el campo fluido puede ser dividido en tres regiones bien diferenciadas (ver figura 1.4): la gota, donde el líquido se acelera debido a la presencia de gradientes de presión; la *lamella*, una delgada lámina de líquido que es eyectada de forma tangente al sustrato desde la región de la gota y donde los gradientes de presión se pueden despreciar debido a su esbeltez; y el *rim*, el extremo de la *lamella* que avanza en dirección radial y limita el perímetro de la gota en expansión [16].

Estos procesos de expansión y rotura de la gota son descritos en términos de parámetros adimensionales. Los más comunes, y que serán los empleados a lo largo de esta tesis para caracterizar los distintos fenómenos observados, son los números de Weber, Reynolds y Ohnesorge. El número de Weber mide la importancia relativa entre la presión dinámica y la presión capilar. El número de Reynolds representa la relación entre las fuerzas de inercia y viscosas usando como velocidad característica la velocidad de impacto. Por último, el número de Ohnesorge se define como el inverso del número de Reynolds cuando se toma como velocidad característica la velocidad capilar.

En cuanto a la caracterización de la superficie, atendiendo a las propiedades de mojabilidad, se pueden diferenciar dos tipos de sustrato en función del valor del ángulo de

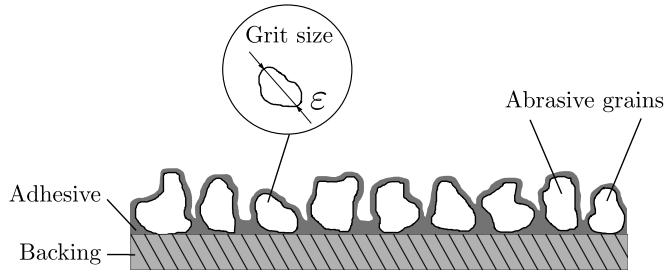

Figura 1.6 Esquema explicativo de la definición del tamaño de grano, ε, de una superficie rugosa, que será el parámetro empleado en esta tesis para caracterizar las irregularidades del sustrato.

contacto, θ, que está relacionado con el grado de repelencia al agua. En la figura 1.5 se puede ver una gota del mismo líquido (agua) depositada sobre dos superficies distintas. Los sustratos en los que el líquido forma un ángulo agudo con la pared se denominan hidrofílicos, mientras que si $\theta > \pi/2$ la superficie se considera hidrófoba.

Por otra parte, la definición de la rugosidad de un sustrato es muy variada en la literatura. Muchos autores emplean la rugosidad media, R_a, un parámetro muy conocido que representa el valor medio de la altura de los distintos puntos de la superficie respecto al plano medio de elevación del sustrato [13, 15, 17, 18]. Pero hay otros autores que prefieren usar parámetros menos comunes como el R_{pk} o altura media de los picos que sobresalen del núcleo de la superficie; la media cuadrática del valor de la ordenada a lo largo de la longitud analizada, R_{rms}; o el espesor medio de las irregularidades, R_{sm}, definido como la media de las longitudes de los picos o valles que conforman la superficie [14, 19, 20]. En esta tesis se empleará el tamaño de grano, ε, que se refiere al diámetro medio de las partículas abrasivas que conforman las superficies rugosas de las lijas que se usarán en el estudio experimental, ya que es un valor proporcionado directamente por el fabricante, véase la figura 1.6. De esta manera, las imperfecciones del sustrato quedan definidas con una única longitud, mientras que en otros casos es necesario conocer dos longitudes para determinar el parámetro que define la rugosidad: la altura de los picos, y la separación entre ellos.

Además, aunque algunos estudios se han centrado en el análisis del efecto de la rugosidad empleando muestras creadas mediante técnicas de microfabricación donde la distribución espacial y la geometría de las protuberancias están definidas y controladas [21–26], esta tesis se enfocará en el análisis de superficies con una distribución arbitraria de las imperfecciones, que son las que se encuentran más habitualmente en las diversas aplicaciones en las que una gota impacta contra un sustrato rugoso.

1.2 Experimentos

Con el objeto de comparar y validar los resultados teóricos de los modelos propuestos, en esta tesis se ha utilizado un montaje experimental como el mostrado en la figura 1.7. Una gota con radio R se deja caer desde una aguja con una velocidad V que puede ser modificada

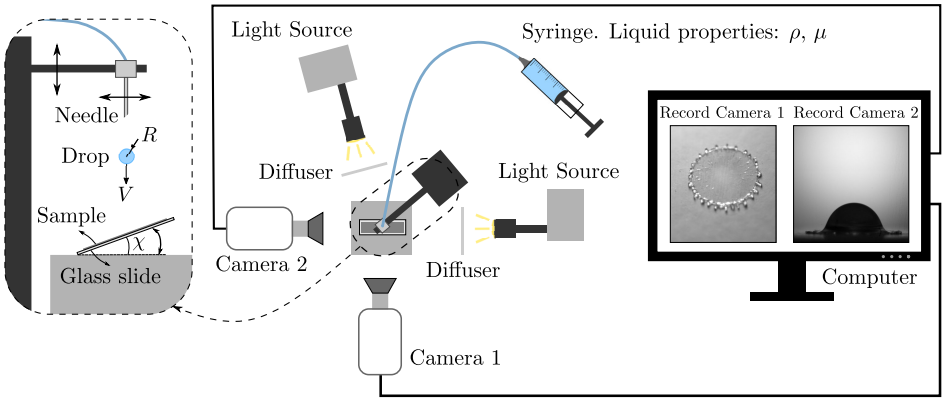

Figura 1.7 Esquema del montaje experimental empleado para realizar los distintos experimentos reportados a lo largo de esta tesis.

variando la altura de caída con respecto a la posición del sustrato sólido. Para ello se bombea un líquido de viscosidad μ y densidad ρ con la ayuda de una jeringuilla de tal modo que la generación de la gota sea cuasiestática. La gota impacta sobre una placa de vidrio cuya superficie puede ser alterada a voluntad, bien aplicando un tratamiento superhidrofóbico o bien solapando lijas de rugosidad controlada y variable. En cualquier caso, estas placas de vidrio, modificadas o no, son siempre sustituidas tras cada experimento. Por último, el ángulo de inclinación χ que forma la superficie de impacto con la horizontal, puede ser variado mediante la ayuda de un goniómetro. Los fenómenos de *spreading* y *splashing* son grabados empleando sendas cámaras de alta velocidad, que graban de manera simultánea los primeros instantes del impacto desde dos vistas diferentes: una lateral y otra cenital. La vista lateral es empleada para determinar el radio y la velocidad de impacto de la gota, mientras que la visión cenital proporciona información cualitativa y cuantitativa de los fenómenos de expansión y rotura de la gota. El posprocesado de las observaciones experimentales se realiza utilizando las herramientas de análisis de imagen incorporadas en el software comercial `MATLAB`.

1.3 *Spreading*

Cuando la velocidad de impacto es baja, la gota, en lugar de disgregarse, mantiene su integridad y se expande sobre la superficie. Si el impacto es perpendicular al sustrato, el proceso de *spreading* es axilsimétrico, pero cuando la trayectoria que sigue la gota forma un ángulo con la pared, situación que se da en la mayoría de casos en los que una gota impacta contra una superficie, la expansión del líquido es asimétrica, véase la figura 1.8 [27–31].

En el caso del impacto normal, el proceso de *spreading* ya ha sido completamente definido en contribuciones previas. Concretamente Gordillo *et al.* [16] desarrollaron un modelo teórico basado en las ecuaciones de balance de masa y de cantidad de movimiento capaz de describir la física del fenómeno de *spreading* y de reproducir los resultados

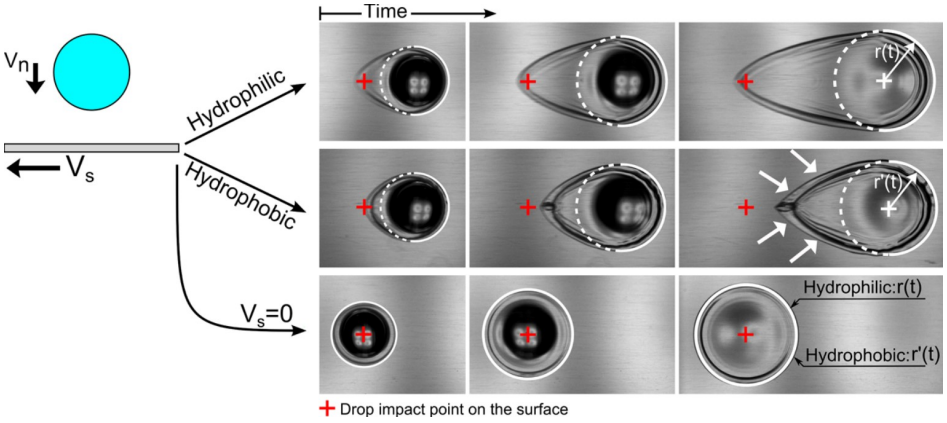

Figura 1.8 Proceso de expansión de una gota de agua con glicerina de radio $R \simeq 1.25$ mm al impactar contra una superficie de acero inoxidable sin tratar, o con un tratamiento hidrofóbico. En las dos primeras filas de imágenes el sustrato se mueve con una velocidad V_s dando lugar a figuras asimétricas, proceso semejante al caso de una gota impactando formando una trayectoria inclinada antes de chocar contra el sólido horizontal y quieto (veáse la figura 1.9). Sin embargo, cuando el sólido está en reposo, en las imágenes de la tercera fila se observa una expansión axilsimétrica con geometrías concéntricas en torno al punto de impacto. Imagen tomada de la referencia [27].

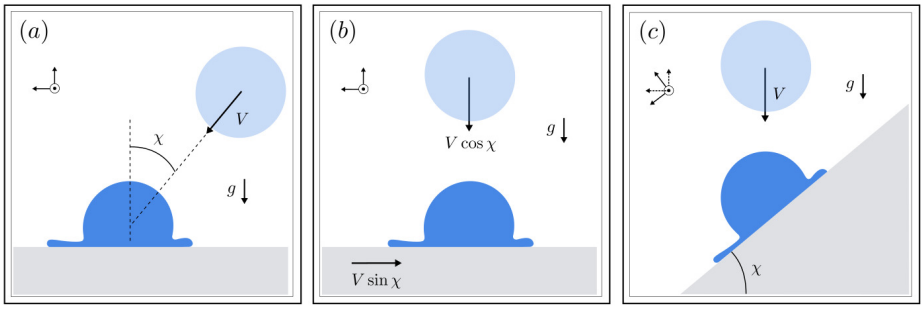

Figura 1.9 Esquema de los distintos tipos de de impacto inclinado abordados en esta tesis así como en otras contribuciones. (a) Impacto de una gota cuya trayectoria forma un ángulo χ con la normal a la superficie. (b) Impacto de una gota sobre una superficie que se traslada paralelamente a sí misma con una velocidad $V \sin\chi$. (c) Impacto vertical sobre una superficie inclinada que forma un ángulo χ con la horizontal.

experimentales de la expansión de una gota a lo largo del tiempo en sustratos horizontales de distinta mojabilidad.

De entre las investigaciones que han tratado el caso del impacto inclinado de gotas sobre

superficie sólidas se observan dos modos diferentes de abordar el problema: colocando el sustrato de forma perpendicular a la dirección de la gravedad o no. En el primer caso, se puede dar a su vez dos situaciones: una gota que cae sobre un sustrato horizontal describiendo una trayectoria que no es perpendicular al mismo (ver figura 1.9a), o una gota impactando verticalmente sobre un sustrato horizontal que se encuentra en movimiento con una determinada velocidad tangencial (ver figura 1.9b). Esta última es la idea que se ha utilizado en el montaje experimental de muchas de las contribuciones presentes en la literatura [27–31]. Sin embargo, en otros estudios [32–35] así como en esta tesis, el impacto inclinado se ha estudiado para el caso de una gota que cae verticalmente sobre un sustrato colocado formando un cierto ángulo sobre la horizontal, fenómeno en el cual la dirección de la gravedad no es perpendicular al sólido, como se muestra en la figura 1.9c. De entre todos ellos, este es el montaje experimental más sencillo a la hora de realizar experimentos de impacto inclinado.

Es importante destacar que, como el tiempo característico del fenónemo de *spreading* es tan corto (de tan solo unos milisegundos), la gravedad no tiene tiempo suficiente para modificar la velocidad del flujo durante el impacto. Además las fuerzas capilares sobre el *rim* son mucho mayores que las fuerzas gravitatorias. Por lo tanto, se pueden despreciar los efectos gravitacionales en la descripción del proceso de expansión de la gota, y los tres sistemas mostrados en la figura 1.9 pueden ser abordados usando el mismo modelo teórico.

A pesar de encontrar en la literatura correlaciones que son capaces de describir las formas asimétricas que se producen durante la expansión de una gota tras el impacto inclinado [27,30,31,35], no existe un estudio capaz de explicar y cuantificar los resultados experimentales partiendo de principios básicos y describiendo la física del problema en cuestión. Por lo tanto, el primer objetivo de esta tesis es intentar rellenar este vacío en el conocimiento aportando tanto nuevos datos experimentales así como una teoría, basada en resultados previos, véase la Ref. [16], que reproduce de manera satisfactoria las observaciones experimentales en lo que concierne a la influencia que posee el ángulo de inclinación de la superficie en la huella que deja la gota tras impactar y que puede ser empleada para describir los tres escenarios mostrados en la figura 1.9.

1.4 *Splashing*

Como se indicó anteriormente, se emplea el término de *splash* para caracterizar aquellas situaciones en las que una gota, tras impactar contra una superficie, termina disgregándose en otras más pequeñas.

Como se puede observar en la figura 1.10, el aire atmosférico juega un papel muy importante en este proceso. De hecho, la influencia del gas de la atmósfera circundante en la aparición de *splash* fue descrito por Riboux y Gordillo [37, 38] con un modelo teórico capaz de reproducir con precisión tanto los datos experimentales propios como los publicados por otros autores. Riboux y Gordillo explican que, para que tenga lugar la eyección de gotas en el caso de sustratos hidrofílicos lisos y secos, es necesario que el frente de avance de la *lamella* (el *rim*) se despegue primero de la pared. Son las fuerzas aerodinámicas sobre esta región las que producen una aceleración vertical y, por tanto,

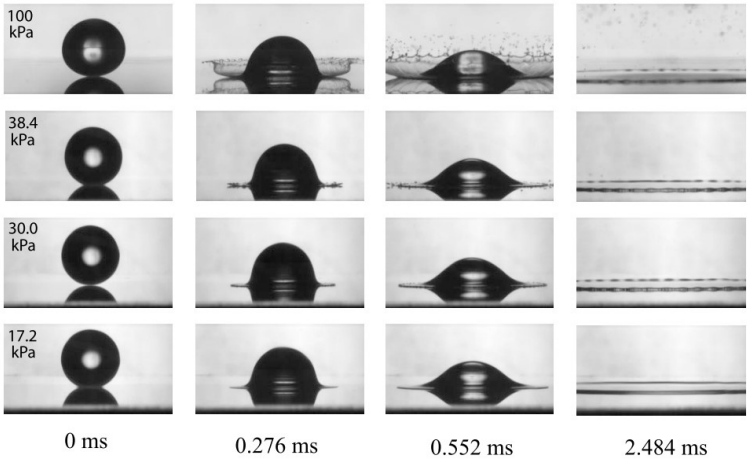

Figura 1.10 Observaciones experimentales del impacto de gotas de etanol sobre placas de vidrio, superficies lisas e hidrofílicas, en distintas condiciones de presión del gas circundante indicadas en cada secuencia de imágenes. Se muestran cuatro instantes de tiempo diferentes: $t = 0$, 0.276, 0.552 y 2.484 ms desde el momento del impacto. Las gotas tienen un radio $R \simeq 1.7$ mm y caen sobre el sólido a la misma velocidad, $V \simeq 3.74$ ms. Imágenes tomadas de la referencia [36].

inducen una velocidad vertical al *rim* que hace que éste que se despegue del sustrato. Una vez que esto ocurre, las inestabilidades capilares pueden crecer en la dirección acimutal del borde de la *lamella*, que termina rompiéndose en gotas que son eyectadas radialmente hacia fuera de la región de impacto.

Pero no todas las superficies son lisas e hidrofílicas. De hecho, ninguna superficie puede considerarse perfectamente lisa. Atendiendo al efecto de las imperfecciones del sustrato en el fenómeno de desintegración de la gota, se ha observado experimentalmente que cuanto mayor es la amplitud de las rugosidades, menor es la velocidad crítica de transición al *splash*, véase la figura 1.11 [12–15, 17–19, 39, 40]. Sin embargo, hasta la publicación de los resultados contenidos en esta tesis, no existía una teoría basada en principios físicos fundamentales que describiese la influencia que tienen las irregularidades de la superficie en el proceso de rotura de una gota al impactar contra una superficie, ni siquiera en condiciones de presión atmosféricas.

Además, existen muchos tipos de superficies que repelen el contacto con el líquido, lo que en la literatura se conoce con el nombre de sustratos hidrofóbos o superhidrofóbos. Este tipo de superficies cada vez son más comunes debido al creciente interés que suscitan por sus diversas aplicaciones prácticas. En efecto, la huella que queda al impactar una gota sobre este tipo de sustratos es menor que sobre una superficie hidrofílica, véase la figura 1.12. Por tanto, las superficies superhidrófobas (es decir, las que repelen el contacto con los líquidos, véase la figura 1.5) se ensucian menos, y tienen mayor capacidad para mantenerse secas y aisladas térmicamente, véase la figura 1.12. Una de las razones que

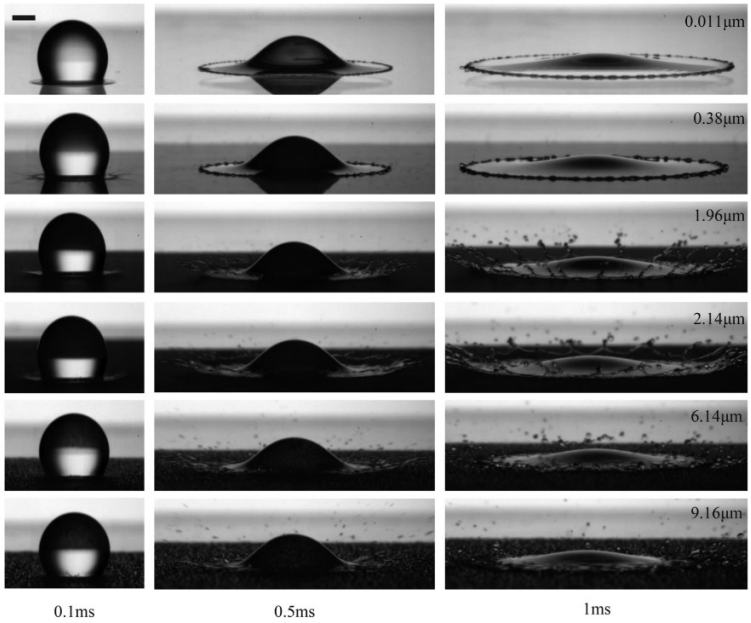

Figura 1.11 Observaciones experimentales de una gota de agua de radio $R \simeq 1.6$ mm impactando a la misma velocidad, $V = 4.1$ m/s, sobre lijas de rugosidad variable, estando indicado el valor de R_a en cada secuencia de imágenes. El tamaño de las imperfecciones va en aumento desde la primera fila hacia abajo. Cada columna corresponde a un mismo instante de tiempo $t = 0.1$, 0.5 y 1 ms después del momento del impacto. La barra de escala es 1 mm. Imagen tomada de la referencia [15].

explican que la mancha que permanece sobre el sólido sea menor, es el hecho de que la velocidad crítica de transición al *splash* disminuye a medida que el ángulo de contacto estático aumenta [19, 42, 43]. Además, el valor del ángulo de contacto estático es, a su vez, una función del tipo de material y también de la rugosidad de la superficie. De hecho, cuando un sustrato es de un material repelente al agua, si además presenta rugosidades, este carácter hidrofóbico se verá fomentado ya que la presencia de protuberancias facilita el atrapamiento de aire entre las mismas, reduciendo así la fricción con el sólido y aumentando la velocidad con la que flujo avanza sobre la superficie.

El proceso de *splash* en superficies repelentes al agua es diferente que el observado en los sustratos hidrofílicos. En el caso de las superficies superhidrófobas el *rim* no está en contacto con la superficie, ni si quiera para velocidades de impacto por debajo de la crítica, véase la figura 1.13. Por lo tanto, ya no son necesarias las fuerzas de sustentación aerodinámicas para despegar el *rim* de la pared, sino que el único requisito para que se produzca el *splash* es que las inestabilidades capilares se puedan desarrollar sin atenuarse [42, 44]. Quintero *et al.* [42] propusieron un modelo capaz de predecir la velocidad crítica de *splash* para el caso de superficies superhidrófobas. Sin embargo, en la figura 1.14 se

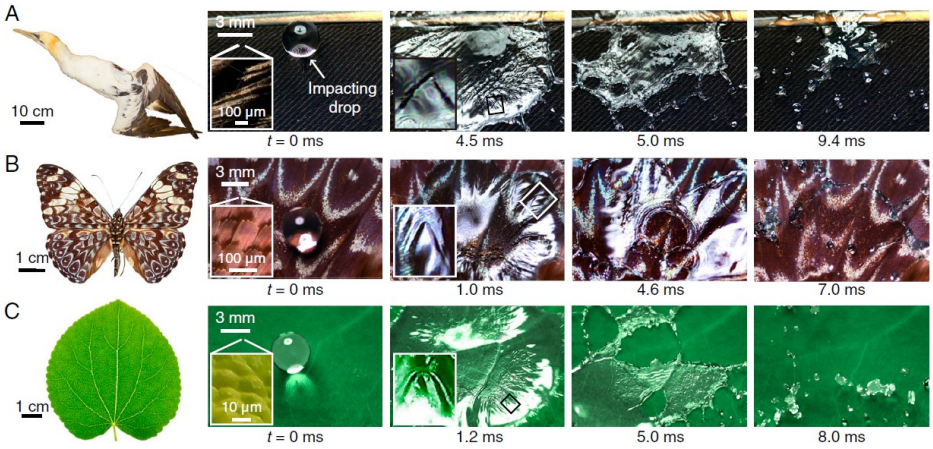

Figura 1.12 Secuencia de imágenes experimentales tras el impacto de una gota de agua de radio $R = 1.7$ mm sobre superficies superhidrófobas presentes en la naturaleza a diferentes velocidades de impacto: A) Pluma de alcatraz, $V = 4.6$ m/s, B) Ala de mariposa, $V = 4.2$ m/s, C) Hoja del árbol de Katsura, $V = 5.4$ m/s. Las imágenes corresponden a distintos instantes de tiempo tras el impacto, indicados en la parte inferior de cada una de ellas. En los cuadros de detalle en $t = 0$ ms se muestran imágenes microscópicas de cada superficie biológica, observándose las microestructuras presentes que confieren a la sólido el carácter superhidrofóbico. Para tiempos superiores, $t > 5$ ms, se aprecia que la gota se ha desintegrado completamente en fragmentos más pequeños [41].

observa que para dos superficies hidrófobas diferentes y dos líquidos de distinta viscosidad no se produce la rotura de la gota a la misma velocidad de impacto. El proceso de *splash* se ve favorecido en el caso con mayor tamaño de las rugosidades, así como la menor viscosidad del líquido. Este efecto no está incluido en el modelo de Quintero *et al.* [42] y, por tanto, motivado por las observaciones experimentales de la figura 1.14, otro de los objetivos de esta tesis será incluir el efecto del tamaño de las rugosidades así como la influencia de la viscosidad del líquido en el modelo de la transición al *splash* propuesto en la referencia [42].

De forma global, el segundo objetivo de esta tesis será analizar detalladamente y ser capaz de predecir mediante modelos analíticos basados en la física que subyace a este problema, la velocidad crítica de *splash* cuando una gota impacta contra superficies de distintas rugosidades y mojabilidades a presión ambiente. El fin es aunar los distintos criterios de *splash*, bien elaborando nuevas teorías o bien introduciendo el efecto de los parámetros de rugosidad y mojabilidad en los modelos previos [37, 38, 42] con el objeto de poder predecir la transición de *spreading* a *splashing* para todo tipo de superficies: sólidos lisos, rugosos, hidrofílicos, hidrofóbicos, así como sustratos superhidrofóbicos, e incluso también para el caso de gotas impactando en el régimen de Leidenfrost, en el que el líquido impacta sobre una superficie caliente tal que el líquido se evapora generándose

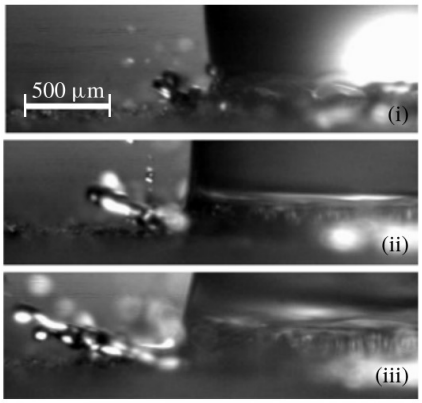

Figura 1.13 Imágenes de una gota de agua de radio $R \simeq 1.5$ mm impactando contra un placa de vidrio a la que se le ha aplicado un tratamiento superhidrofóbico para distintas velocidades de impacto, tanto inferiores al valor crítico: (i) $V \simeq 1.7$ ms, como velocidades en el régimen de *splash*: (ii) $V \simeq 2.1$ ms, y (iii) $V \simeq 2.6$ ms. El *rim* se encuentra en todo momento separado de la pared, independientemente del valor de la velocidad de impacto. Imágen tomada de la referencia [42].

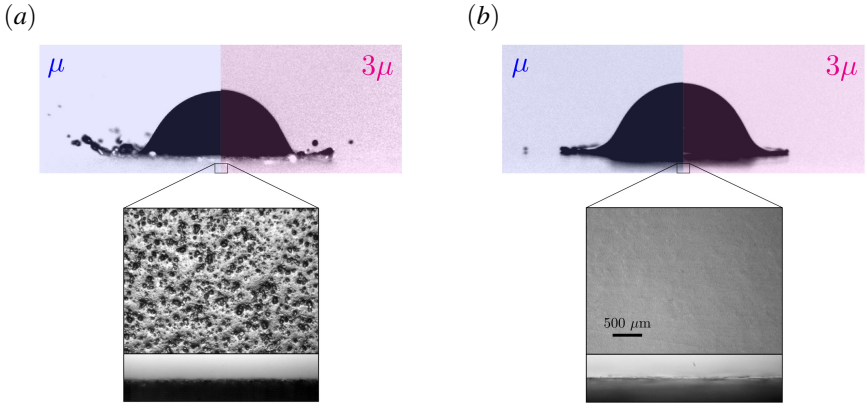

Figura 1.14 Imágenes experimentales de una gota de agua (fondo azul) o de un líquido tres veces más viscoso, agua con azúcar al 30 % en masa (fondo rosa), impactando sobre superficies hidrófobas de distinta rugosidad: (a) Placa de vidrio con tratamiento superhidrofóbico, $\varepsilon = 60 \pm 40$ μm, (b) sustrato de Teflón liso, $\varepsilon \sim 0$. La velocidad de impacto es aproximadamente la misma en ambos casos, $V \simeq 2.5$ m/s.

una fina lámina de vapor que evita que la gota entre en contacto con el sustrato.

En conclusión, en esta tesis se proporciona una descripción teórica, avalada por datos experimentales, que permite describir el proceso de expansión de una gota sobre una superficie inclinada. Asimismo, también se proporcionarán ecuaciones que permiten predecir la velocidad crítica de transición al *splash* como función de la mojabilidad y de la rugosidad del sustrato, clasificando los distintos tipos de superficies en función de su rugosidad superficial y del valor del ángulo de contacto, pues cuanto mayores sean estos valores, mayor será la cantidad de aire atrapado entre la gota y el sustrato y, por tanto, menores serán las velocidades críticas de *splash*.

2 Inclined impact of drops

Here we extend the results in Gordillo *et al.* [16], where the spreading of drops impacting perpendicularly a solid wall was analysed, to predict the time-varying flow field and the thickness of the liquid film created when a spherical drop of a low viscosity fluid, like water or ethanol, spreads over a smooth dry surface at arbitrary values of the angle formed between the drop impact direction and the substrate. Our theoretical results accurately predict the time evolving asymmetric shape of the border of the thin liquid film extending over the substrate during the initial instants of the drop spreading process. In addition, the particularization of the ordinary differential equations governing the unsteady flow when the rim velocity vanishes provides an algebraic equation for the asymmetric final shapes of the liquid stains remaining after the impact, valid for low values of the inclination angle. For larger values of the inclination angle, the final shape of the drop can be approximated by an ellipse whose major and minor semiaxes can also be calculated by making use of the present theory. The predicted final shapes agree with the observed remaining stains, excluding the fact that a liquid rivulet develops from the bottom part of the drop. The limitations of the present theory to describe the emergence of the rivulet are also discussed.

En este capítulo se propone un modelo capaz de predecir el campo de velocidades y el espesor de la lámina de líquido que surge cuando una gota de un líquido de baja viscosidad (ej. agua o etanol) impacta y se expande sobre una superficie lisa y seca, para distintos valores del ángulo que forma la dirección de impacto de la gota y el sustrato. Para ello se realiza una extensión de la teoría de Gordillo *et al.* [16], que describe la expansión de gotas al impactar perpendicularmente sobre una pared sólida. Durante los instantes iniciales del proceso de *spreading*, los resultados teóricos derivados de este estudio son capaces de predecir de forma precisa la evolución temporal de la posición del extremo de la fina lámina de líquido en expansión, que es asimétrica. Además, las ecuaciones diferenciales ordinarias obtenidas para describir el flujo en la *lamella* se particularizan en el instante en el que la velocidad del *rim* es nula, dando lugar a una ecuación algebraica empleada para definir la forma final de la mancha de líquido que permanece en la pared

tras el impacto. Esta expresión es válida cuando el ángulo de inclinación es bajo. Para mayores valores del ángulo de inclinación, la forma final de la gota se puede aproximar a la de una elipse caracterizada por sus semiejes mayor y menor lo cuales también pueden ser calculados haciendo uso de la teoría propuesta. Las formas finales predichas con el modelo propuesto concuerdan con las observaciones experimentales de las manchas de líquido que permanencen en la pared, exceptuando el hecho de que en la parte inferior de la gota se forma una acumulación de líquido que fluye hacia abajo. Las limitaciones de la teoría para describir la aparición de este chorro líquido también se incluyen en este capítulo.

Paper reference:

García-Geijo, P., Riboux, G., & Gordillo, J. (2020). Inclined impact of drops. *Journal of Fluid Mechanics*, **897**, A12. doi:10.1017/jfm.2020.373

Citations: 13 (WoS 2023)
20 (Google Scholar 2023)
14 (Scopus 2023)

FWCI: 1.45 (Scopus 2023)

Journal of Fluid Mechanics:
Impact Factor: 4.245 (JCR 2021)
Category: Physics, Fluids & Plasmas
Category Rank: 3/34 (JCR 2021)
Category Quartile: Q1 (JCR 2021)

Scan the QR code for accessing paper in the publisher website:

3 Spreading and splashing of drops impacting rough substrates

Paper reference:

García-Geijo, P., Quintero, E., Riboux, G., & Gordillo, J. (2021). Spreading and splashing of drops impacting rough substrates. *Journal of Fluid Mechanics*, **917**, A50. doi:10.1017/jfm.2021.313

Open Access

Citations: 18 (WoS 2023)
20 (Google Scholar 2023)
17 (Scopus 2023)

FWCI: 2.79 (Scopus 2023)

Journal of Fluid Mechanics:
Impact Factor: 4.245 (JCR 2021)
Category: Physics, Fluids & Plasmas
Category Rank: 3/34 (JCR 2021)
Category Quartile: Q1 (JCR 2021)

Scan the QR code for accessing paper in the publisher website:

J. Fluid Mech. (2021), *vol*. 917, A50, doi:10.1017/jfm.2021.313

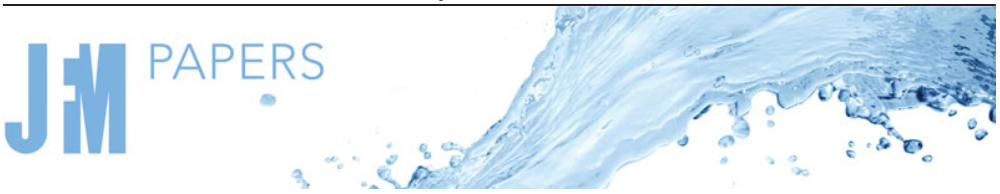

Spreading and splashing of drops impacting rough substrates

P. García-Geijo[1], E. S. Quintero[1], G. Riboux[1] and J. M. Gordillo[1],†

[1] Área de Mecánica de Fluidos, Departamento de Ingeniería Aeroespacial y Mecánica de Fluidos, Universidad de Sevilla, Avenida de los Descubrimientos s/n, 41092 Sevilla, Spain

(Received 30 October 2020; revised 24 February 2021; accepted 6 April 2021)

Here, we present experimental results of water and ethanol drops of radii R, density ρ and interfacial tension coefficient σ, impacting with a velocity V over different types of sandpapers containing particles of characteristic diameter ε embedded in their surfaces. It is shown that the transition from spreading to splashing at normal atmospheric conditions can be classified depending on the value of the parameter $\varepsilon/H_t \simeq We_\varepsilon = We(\varepsilon/R)$, with $We = \rho V^2 R/\sigma$ the Weber number and H_t indicating the initial thickness of the thin film – the lamella – which is ejected along the substrate once the drop touches the solid. When $We_\varepsilon \lesssim 1$ and the liquid wets the substrate, the critical value of the Weber number above which the drop splashes, We_c, can be predicted using the results in Gordillo & Riboux (*J. Fluid Mech.*, vol. 871, 2019, R3) once the angle the advancing rim forms with the substrate, α, is expressed as a decreasing function of the static advancing contact angle. The calculated values of We_c for the case of water drops impacting over rough substrates are smaller than the corresponding ones for smooth substrates, in agreement with experimental observations. Moreover, if the liquid does not wet the substrate, it is also shown that the splash velocity can be predicted using the theory for superhydrophobic substrates in Quintero, Riboux & Gordillo (*J. Fluid Mech.*, vol. 870, 2019, 175–188). For those cases in which $We_\varepsilon \gtrsim 1$ and the liquid wets the substrate, we demonstrate that the critical Weber number for splashing decreases with ε as $We_c \propto (R\cos\theta_0/\varepsilon)^{3/5}$, with θ_0 the value of the Young contact angle.

Key words: aerosols/atomization, drops

† Email address for correspondence: jgordill@us.es

1. Introduction

A drop impacting a dry solid substrate will either spread tangentially to the surface without breaking or will splash, disintegrating into tiny droplets ejected radially outwards at velocities far larger than the impacting one (Yarin 2006; Josserand & Thoroddsen 2016). It is now known that the conditions under which splashing occurs does not only depend on the liquid properties, on the impact velocity and on the drop radius, as expressed by the well-known correlation proposed in Mundo, Sommerfeld & Tropea (1995), but also on other parameters such as the surrounding gas pressure (Xu, Zhang & Nagel 2005; Riboux & Gordillo 2014; Stevens 2014; Gordillo & Riboux 2019), the roughness (Stow, Hadfield & Ziman 1981; Range & Feuillebois 1998; Xu, Barcos & Nagel 2007; Latka *et al.* 2012; Quetzeri-Santiago, Castrejón-Pita & Castrejón-Pita 2019*a*) or the substrate wettability (de Goede *et al.* 2018; Quetzeri-Santiago *et al.* 2019*b*; Quintero, Riboux & Gordillo 2019), with wetting and roughness intimately related with each other, see e.g. Quéré (2008).

It is the purpose of this contribution to analyse the spreading and splashing of droplets of low viscosity liquids such as water and ethanol or mixtures of both impacting at normal atmospheric conditions over rough substrates. These are, precisely, the most common conditions involving the impact of a drop against a solid found in both practical applications and in our daily life experience: indeed think, for instance, of rain drops falling on the sidewalk, which clearly is a rough substrate like the vast majority of solids. Our study will be limited to analysing those cases in which the surface is initially dry, a situation which differs from the similar – albeit simpler case because neither the topography of the substrate nor wetting effects are present – in which the drop falls on a pool or thin liquid film (Josserand & Zaleski 2003; Cimpeanu & Moore 2018). It will also be assumed that the drop falls over the solid perpendicularly because the effects associated with the impact direction (Bird, Tsai & Stone 2009; Almohammadi & Amirfazli 2017; Hao & Green 2017; Hao *et al.* 2019) can be easily accounted for using the framework put forward in, for instance, Gordillo & Riboux (2019) and García-Geijo, Riboux & Gordillo (2020).

As it was mentioned above, Mundo *et al.* (1995) studied the case of drops impacting at normal atmospheric conditions on either smooth or rough dry surfaces and characterized the spreading–splashing transition through the so-called K parameter, or splashing parameter, which is nothing but a correlation involving the Reynolds and Ohnesorge numbers based on the liquid properties. Nevertheless, the experiments conducted by Xu *et al.* (2005) and Stevens (2014) revealed that drop splashing can be suppressed by reducing the air pressure and also that the splash threshold velocity behaves non-monotonically for low values of atmospheric pressure, these facts indicating that drop splashing heavily depends on the properties of the surrounding gaseous atmosphere. The correlation found by Mundo *et al.* (1995), as well as the experimental results found by Xu *et al.* (2005) and Stevens (2014), were reconciled by the theory presented in Riboux & Gordillo (2014) and Gordillo & Riboux (2019), where it is shown that the splashing of drops is produced by the lift force exerted by the air on the edge of the lamella. The ideas in Riboux & Gordillo (2014) were developed for the case of smooth dry substrates, and it will be one of the purposes in this contribution to check whether they can also be applied to the case of rough solids or not.

In their now classical contribution, Stow *et al.* (1981) analysed the splashing of drops on rough substrates, observing that the critical velocity for splashing decreases with increasing values of the amplitude of the roughness. Stow *et al.* (1981) also proposed a correlation based on the Reynolds (Re) and Weber (We) numbers and on the surface roughness in order to fit their experimental data and, later on, the experiments reported

in Rioboo, Tropea & Marengo (2001) and Range & Feuillebois (1998) confirmed the observations in Stow *et al.* (1981) that the critical Weber number for splashing depends on the amplitude of the substrate roughness. More recently, Roisman, Lembach & Tropea (2015) proposed a correlation expressing that the critical Weber number for splashing does not depend on the roughness amplitude but on the slope of the substrate corrugations. In the same vein, but for the case of microstructured surfaces, Xu (2007), Tsai *et al.* (2010), Lembach *et al.* (2010), Kim *et al.* (2014), de Jong, Enríquez & van der Meer (2015) and Yarin, Roisman & Tropea (2017) showed that the transition from spreading to splashing depends on the geometrical arrangement of the micropillars. The influence of both air pressure and surface roughness on drop splashing was analysed experimentally by Xu *et al.* (2007) and Latka *et al.* (2012), who found that both aerodynamic forces and the substrate roughness play a role in the splashing of drop, but they did not provide with any type of fit, correlation or theory to quantify their observations. In addition, Josserand *et al.* (2005) simulated the effect on drop splashing of a single obstacle placed on an otherwise dry and smooth substrate and compared the numerical results with experimental observations.

The previous revision reveals that there is a lack of physical understanding of the role played by the surface corrugations in triggering the splash, even at normal atmospheric conditions. Then, based on our own experimental observations, here, we present simplified models which, retaining the underlaying physics, provide with predictions for the splash threshold velocity at normal atmospheric conditions, in good agreement with observations. In addition, it will be shown that the equations describing the spreading of drops deduced in Gordillo, Riboux & Quintero (2019) can also be used to predict the observations with rough substrates. While Rioboo *et al.* (2001), Xu *et al.* (2007), Latka *et al.* (2012) and Hao (2017) establish a difference between two types of splashing namely, prompt splashing and corona splashing, here, we will make no distinction between them and will simply determine the conditions for which the drops keep their integrity after the impact (spreading) or they break into smaller and faster droplets (splashing). Let us point out here that this study focuses on the most common case of applications in which neither the spatial distribution nor the geometry of the protuberances of the rough substrate are controlled using microfabrication techniques.

The paper is structured as follows: in § 2 we describe the set-up and present the experimental results, § 3 is devoted to providing the theoretical models for the spreading and the splashing of drops and to showing comparisons of the predictions with the experimental observations. The main conclusions are presented in § 4.

2. Experimental set-up and phenomenology

Figure 1 is a sketch of the experimental set-up used to produce water or ethanol drops of radii R impacting over different types of sandpapers, these being replaced after each measurement. The drops produced in this way fall with a variable and controllable velocity V within the range of values indicated in table 1. The side and top views of the drop impact process are extracted from the analysis of the videos recorded using two different high-speed cameras: figure 1 shows that a Phantom V710, operated at 33 000 f.p.s. (frames per second) is used to get the images from above with a spatial resolution of 42 μm per pixel, whereas a Phantom V7.3, operated between 11 000 and 13 000 f.p.s. is employed to get the lateral views with a spatial resolution of $\sim$18 μm pixel^{-1}. With the purpose of analysing the effect of wettability on the spreading to splashing transition, two different types of substrates have been employed: here, we make use of high quality silicon-carbide sandpapers with either paper or cloth backing and of aluminium-oxide lapping films

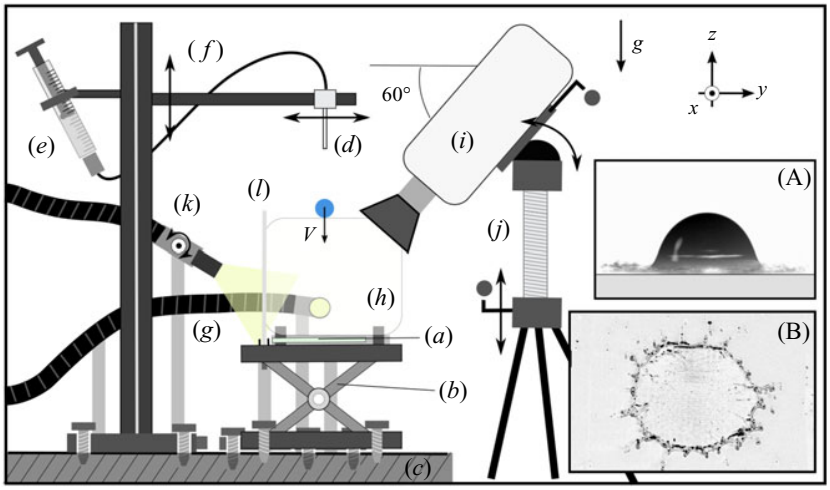

Figure 1. Sketch of the experimental set-up used to record the side views of the falling drops (A) and also the views from the top of the spreading or splashing processes (B). The set-up consists of a glass slide Knittel 76 × 26 mm (*a*) to which a portion of sandpaper is fixed thanks to double-sided scotch film. The sample is removed and replaced after each experiment. The glass slide is placed at a constant height over a vertical travel L200 Thorlabs Lab Jack (*b*) which is rigidly fixed to a non-vibrating table Photon Control (*c*). Drops are produced quasi-statically injecting either water or ethanol through a Biolin Scientific C209-22 metallic needle of outer diameter ∼0.7 mm (*d*) by means of a 1 ml threaded plunger glass syringe Hamilton model 81 441 (*e*). The height of the injection needle and, hence, the drop impact velocity V, can be changed by means of Standard Thorlabs rails (*f*). Experimental images are recorded using two different high-speed cameras. A Phantom camera V7.3, which is not shown in the sketch, is coupled with an objective Edmund Industrial Optics 4× pointing in the direction of a light source Schott KL2500 LCD (*g*), aligned with the x axis of the sketch; a light diffuser Thorlabs DG100x100 (*h*) is used to improve the quality of the images obtained. The images recorded in this way are of the type shown in (*A*). A second camera Phantom V710 with a Sigma 105 mm DG Macro objective (*i*) records the type of images depicted in (*B*). It is mounted in a tripod Manfrotto Model #028 (*j*), used to either rotate the camera around the x direction or to move the camera along the z axis in the sketch. The images recorded using this second camera are illuminated thanks to a second light source, emitted by a Schott KL2500 LCD (*k*) which passes through a Thorlabs diffuser DG100x100 (*l*), placed in the plane (x–z).

with polyester backing, hereinafter denoted as SC and AO sandpapers, respectively. The substrate roughness will be characterized by means of the so-called grit size ε, which refers to the average diameter of the abrasive particles embedded in the surface, as shown in figure 2(*a*), because this value is provided directly by the manufacturers. The values of the grit sizes for SC sandpapers are usually characterized by the European standard FEPA (Federation of European Producers of Abrasives), which is identical to the ISO (International Organization for Standardization) standard, while those for AO sandpapers are indicated through its colour, see table 1. The measurement of the substrate roughness through the grit size ε differs from that used by Range & Feuillebois (1998), Xu *et al.* (2007), Tang *et al.* (2017) and Hao (2017), who employed R_a, see figure 2(*a*), or by Latka *et al.* (2012), Quetzeri-Santiago *et al.* (2019*a*) and Roisman *et al.* (2015), who made use of other parameters such as R_{pk} or the root mean square roughness, R_{rms}.

The relationship between R_a and the grit size ε has been determined here by performing measurements using samples of all types of AO sandpapers listed in table 1 as well as the finest SC substrates. In these type of experiments, where ε is known, different images of the substrate topography have been recorded using a laser scanning confocal microscope, see figure 2(*b*). The images obtained in this way have been later on analysed by means of

Sandpaper	ε (μm)	R_a (μm)	f	S_{dq}	We Water	We Ethanol	θ	θ_{rec}	θ_{adv}	θ_0
SC P220	68	10.07	∼3	—	43–265	64–376	$32 \pm 5^\circ$	21°	54°	73°
	—	—	—	—	—	—	$56 \pm 6^\circ$	49°	69°	79°
SC P500	30	4.97	∼3	—	42–256	64–382	$65 \pm 3^\circ$	54°	76°	81°
SC P1000	18	3.36	∼3	—	43–256	64–391	$74 \pm 1^\circ$	61°	76°	84°
SC P2400	9	2.15	2.40	5.30	36–242	68–377	$31 \pm 4^\circ$	27°	44°	69°
SC P4000	5	1.61	2.61	5.22	37–223	64–370	$98 \pm 2^\circ$	75°	122°	SH
SC P6000	4	1.48	2.66	6.19	40–225	—	$97 \pm 4^\circ$	71°	124°	SH
SC P8000	3	1.35	2.66	5.17	39–225	—	$100 \pm 6^\circ$	80°	135°	SH
AO Green	30	4.97	2.77	8.83	38–269	—	$41 \pm 2^\circ$	7°	40°	74°
AO Blue	9	2.15	2.26	4.77	37–269	—	$28 \pm 3^\circ$	10°	41°	67°
AO Pink	3	1.35	2.03	3.81	37–267	—	$43 \pm 2^\circ$	8°	42°	69°
AO Lime	1	1.08	1.06	0.40	35–267	—	$70 \pm 2^\circ$	66°	95°	71°
AO White	0.3	0.30	1.08	0.46	34–265	—	$90 \pm 4^\circ$	76°	102°	90.0°

Table 1. In this experimental study, two different types of liquids, water and ethanol, have been employed. The radii of the drops do not vary much for each of the two liquids used and, consequently, in this contribution we will take the constant values $R = 1.44$ mm for water drops and $R = 1.05$ mm for ethanol drops. Using these values of R and of the standard material properties for water and ethanol at 25 °C, the values of the Ohnesorge number defined in (2.4*a–d*) are constant for each of the two liquids and equal to $Oh = 3.1 \times 10^{-3}$ for the case of water and $Oh = 7.3 \times 10^{-3}$ for the case of ethanol. However, the value of the Weber number, We, defined in (2.4*a–d*) is varied within the ranges indicated in the table. The roughnesses of the two types of sandpapers employed here are classified using the grit size, following the FEPA/ISO designation for SC sandpapers and the surface colour for AO sandpapers. The given values of ε and those of R_a calculated using (2.1) are provided in the table, as well as the values of the roughness ratio f and of the dimensionless parameter measuring the slope of the corrugations, S_{dq}, defined in (2.2). For the case of water drops and for each of the two types of sandpapers used, the table includes the values of the macroscopic static contact angle θ, which is measured from high resolution images taken at the scale of the drop, which is much larger than the grit size. For the case of water drops, the values of the Young angle θ_0, of the advancing θ_{adv} and of the receding θ_{rec} contact angles are also provided in the table. The values of θ_0 are calculated using the measured values of θ, as illustrated in figure 3. The values of θ_{adv} and θ_{rec} are measured from high resolution images taken at the instant when drops placed over inclined substrates start sliding at the critical inclination angle (Extrand & Kumagai 1995). For the case of ethanol drops, $\theta \simeq \theta_{adv} \simeq \theta_{rec} \simeq 0$. For the case of the SC P220 our experiments reveal that, indeed, there exists two different possible values of the macroscopic contact angle θ which, consistently, correspond to almost the same value of the Young angle θ_0.

the software SensoMAP Premium 7.4.8114 with the purpose of calculating the value of $R_a = 1/A \iint_A |z(x, y)| \, \mathrm{d}x \, \mathrm{d}y$, with A the sampling area. A least-square fitting reveals that R_a and ε are related with each other through equations

$$\left.\begin{aligned} R_a = 0.943 + 0.134\varepsilon \quad \text{for } R_a \geq 1 \ \mu\text{m}, \\ R_a = \varepsilon \quad \text{for } R_a < 1 \ \mu\text{m}, \end{aligned}\right\} \tag{2.1}$$

with both R_a and ε expressed in μm. Equation (2.1) will be used in what follows to express R_a as a function of ε and *vice versa*. The topography of the rough substrate will also be characterized in terms of the parameter measuring the slope of the corrugations, also given in table 1,

$$S_{dq} = \sqrt{\frac{1}{A} \iint_A \left[\left(\frac{\partial z(x, y)}{\partial x} \right)^2 + \left(\frac{\partial z(x, y)}{\partial y} \right)^2 \right] \mathrm{d}x \, \mathrm{d}y}, \tag{2.2}$$

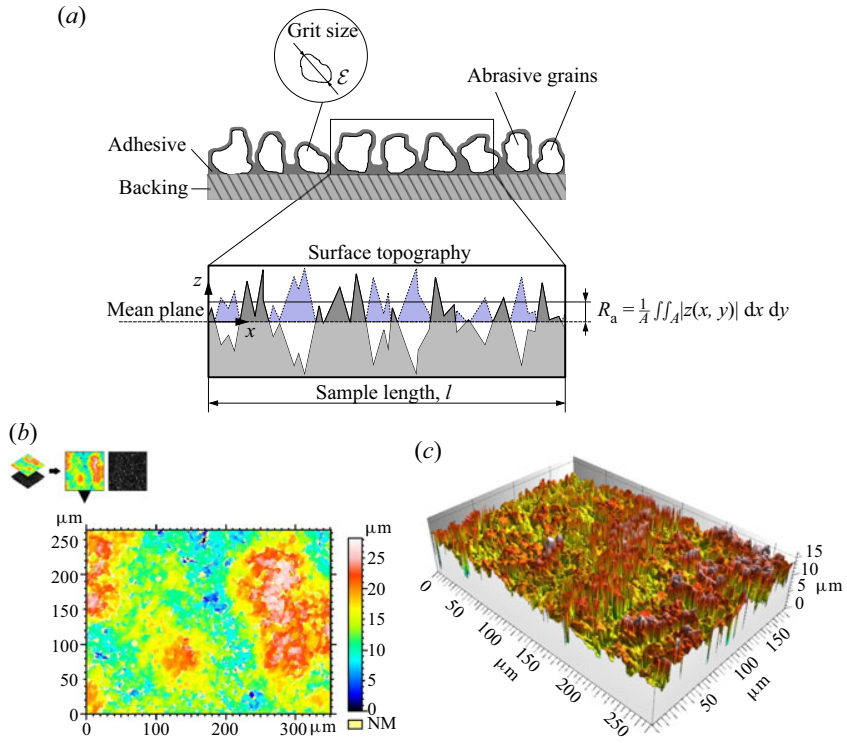

Figure 2. (*a*) Sketch showing two of the different parameters used in this study in order to characterize the surface roughness: the grit size, ε, and the arithmetical mean roughness, R_a. The grit size is provided by the manufacturer since it represents the characteristic diameter of the particles used in the fabrication process, whereas R_a depends on the surface topography. The value of R_a is determined using profilometers or microscopes and it is defined as the average value of the height of each point with respect to the arithmetical mean of the surface elevation throughout the sample length (Gadelmawla *et al.* 2002). The peaks, placed above the mean plane, are represented in dark grey, whereas the absolute values of the ordinates of the points located below the mean plane, are depicted in blue. (*b*) Two- and three-dimensional views of the surface topography corresponding to a sample of P2400 SC sandpaper – see table 1 – obtained by means of the software SensoMAP Premium 7.4.8114 from the analysis of the images obtained with a laser scanning confocal microscope.

where z indicates the elevation of the peaks. Quéré (2008) analysed the set of experiments by Onda *et al.* (1996) and Shibuichi *et al.* (1996) and provided useful equations relating θ, which is the contact angle the liquid forms with a rough surface, with the Young angle θ_0, defined as the static angle the liquid forms with a flat solid made of the same material. For the case the drop rests on the substrate in the Wenzel regime, which is the case for water drops on the sandpapers in table 1 with larger values of ε, the relationship between θ and θ_0 can be expressed as, see Quéré (2008),

$$\cos\theta = f\cos\theta_0, \tag{2.3}$$

with f the roughness factor given in table 1 and in figure 3(*a*), defined as the ratio between the areas of the rough and the flat surfaces. Figure 3(*a*) shows that f increases with $R_a(\varepsilon)$, reaching a plateau for rougher surfaces. Table 1 also reveals that the SC sandpapers with $\varepsilon < 5$ μm, which are fabricated using a cloth backing instead of the paper backing used in the other types of SC sandpapers considered here, possess a superhydrophobic-like (SH) behaviour.

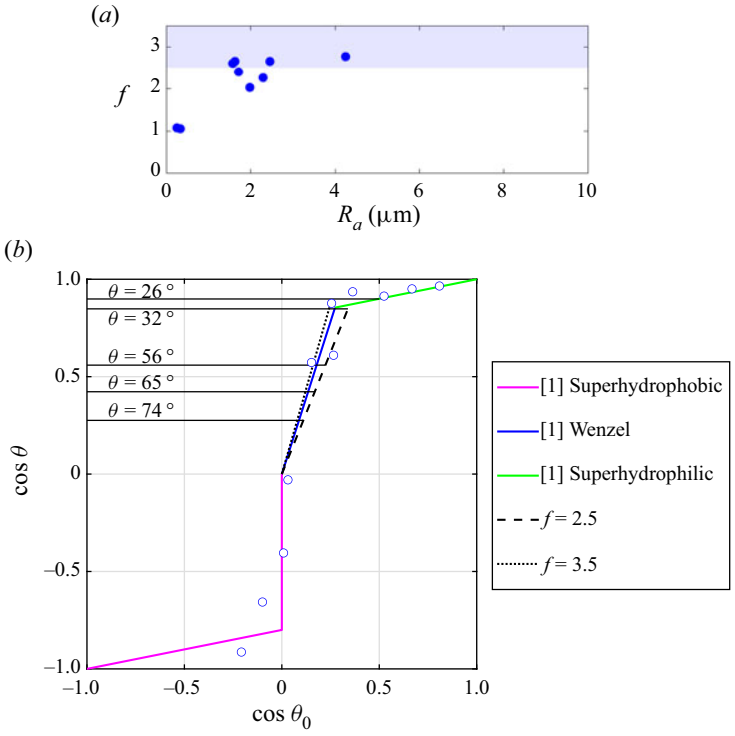

Figure 3. (*a*) Value of the roughness factor f as a function of the measured mean roughness, R_a, for the different types of sandpapers in table 1 with $R_a < 10$ μm. (*b*) Figure adapted from Quéré (2008): the relationship between the cosine of the macroscopic contact angle, θ, and the Young angle, θ_0, can be calculated using the results in [1] of Quéré (2008), obtained analysing the experimental data in Onda *et al.* (1996) and Shibuichi *et al.* (1996), represented with open circles. This figure includes the curves corresponding to the case in which the drop rests on the substrate in the Wenzel regime for two different values of f, whereas the horizontal lines illustrate how θ_0 is calculated using the measured values of θ.

In the remainder of this contribution, lengths, velocities, times and pressures will be made dimensionless using R, V, R/V and ρV^2 as the characteristic values of length, velocity, time and pressure. Therefore, the drop spreading and splashing processes at normal atmospheric conditions will be characterized in terms of the following dimensionless parameters:

$$We = \frac{\rho V^2 R}{\sigma}, \quad Oh = \frac{\mu}{\sqrt{\rho R \sigma}}, \quad Re = \frac{\sqrt{We}}{Oh} \quad \text{and} \quad \epsilon = \frac{\varepsilon}{R}, \tag{2.4a–d}$$

with ρ, μ and σ indicating the liquid density, viscosity and interfacial tension coefficient, respectively. The experimental values of We, ϵ and Oh explored, as well as the values of the macroscopic static contact angle θ, are provided in table 1, where it is also shown that the grit size varies between $\varepsilon \sim 0.3$ and $\varepsilon \sim 68$ μm which results, using (2.1), in values of the mean roughness varying between $R_a \sim 0.30$ and $R_a \sim 10.1$ μm. Let us point out here that, since $\varepsilon \sim 0.014$ μm for the case of smooth glass slides (Hao 2017; Quetzeri-Santiago *et al.* 2019*a*), in the following, the value $\epsilon \sim 10^{-5}$ will be used to characterize the experiments corresponding to millimetric water or ethanol drops falling over smooth substrates. As was already pointed out in the introduction, no distinction will be made between prompt and

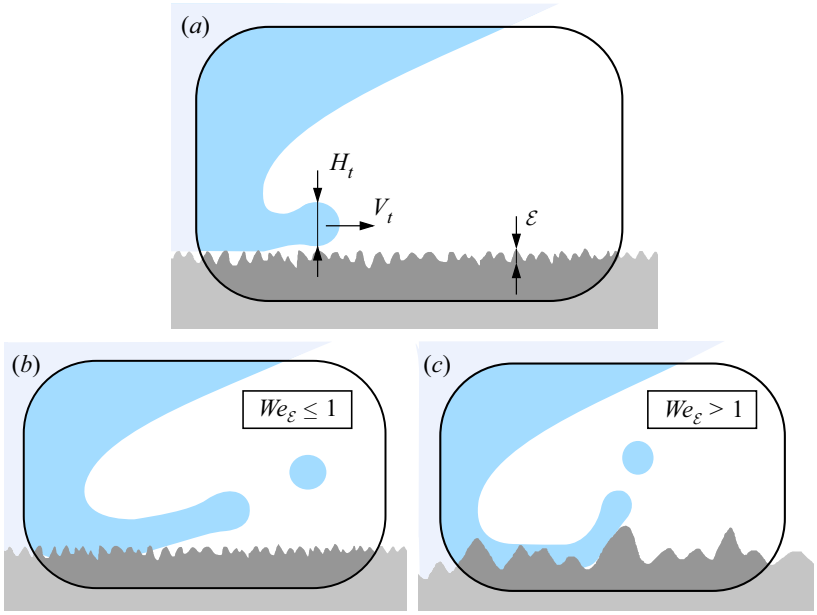

Figure 4. (*a*) Sketch showing the definitions of the initial thickness of the lamella, H_t, as well as the initial velocity of the rim, V_t. The type of splash crucially depends on whether $We_\varepsilon < 1$ namely, $H_t > \varepsilon$ (*b*) or $We_\varepsilon > 1$ namely, $H_t < \varepsilon$ (*c*), see (2.6).

corona splashing and here we will focus on determining the conditions under which the drops keep their integrity and spread or they break and splash, ejecting faster droplets. Usually, whenever the impact velocity is slightly larger than the splash velocity, many tiny droplets can be depicted in the experimental images (Riboux & Gordillo 2015), with the total volume of the liquid ejected increasing with V, as described in Burzynski, Roisman & Bansmer (2020), who quantified their observations in terms of the parameter β defined in Riboux & Gordillo (2014).

Once the experimental set-up has been described and the surface roughness has been characterized in terms of the grit size ε, the rest of the section is dedicated to present the rich phenomenology arising after the impact of a drop on a rough substrate. The analysis of the different experimental information presented next makes use of previous results in Riboux & Gordillo (2014), where it is found that the rim thickness and velocity at the instant the lamella is initially ejected, H_t and V_t respectively – see figure 4 – can be expressed, in the limit of low values of the Ohnesorge number of interest here, in terms of the drop radius R, the impact velocity V and the Weber number defined in (2.4*a–d*) as

$$H_t \simeq RWe^{-1}, \quad V_t \simeq (\sqrt{3}/2)V\,We^{1/3}. \tag{2.5a,b}$$

Equations (2.5*a*,*b*) have been deduced taking into account that $V_t = (\sqrt{3}/2)V\,t_e^{-1/2}$, $H_t = R(\sqrt{12}/\pi)t_e^{3/2}$ and also that, in the limit $Oh \ll 1$, $t_e = 1.05\,We^{-2/3}$, with t_e the dimensionless instant the lamella is initially ejected.

It will be shown next that the ratio between the grit size ε and the thickness of the lamella H_t which, making use of the (2.5*a*,*b*), can be expressed as

$$We_\varepsilon = \frac{\varepsilon}{H_t} = \frac{\rho V^2 \varepsilon}{\sigma}, \tag{2.6}$$

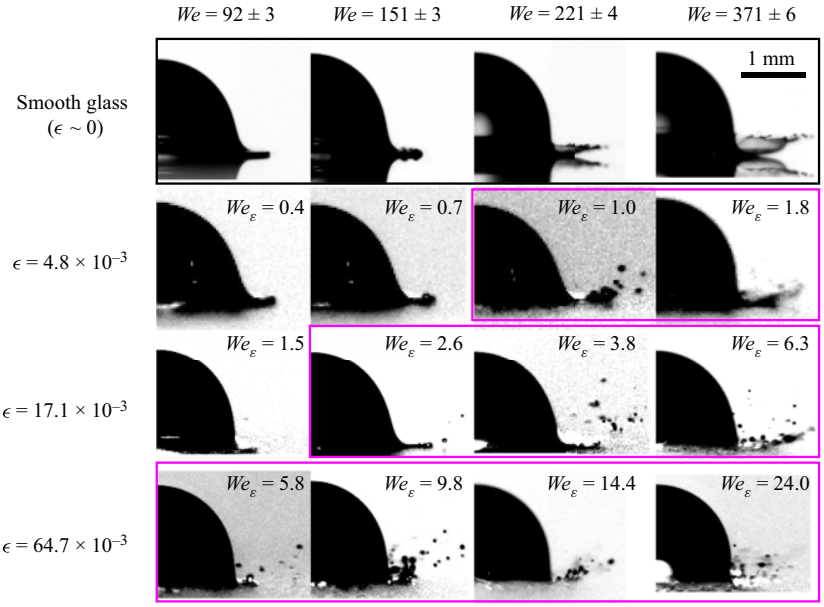

Figure 5. Experimental images showing the impact of ethanol drops over SC sandpapers at the same dimensionless time, $t = TV/R = 0.6 \pm 0.1$ for different values of the parameters We and ϵ defined in (2.4*a–d*). The first row, highlighted in black, corresponds to the case of a smooth glass substrate whereas the rest of the cases correspond to SC sandpapers. The value of We_ε defined in (2.6), which measures the ratio between the grit size ε and the thickness of the lamella H_t – see figure 4 and (2.5*a*,*b*) – is indicated in each of the images. For a given value of ϵ, there exists a value of the Weber number, We_c, to be termed in what follows the critical Weber number for splashing, above which the drop splashes. The splash cases are highlighted in pink. The splash transition can also be triggered increasing ϵ for a given We.

plays an essential role in the splashing behaviour of impacting droplets, see figure 4. Indeed, figure 5, which shows the influence of varying We and ϵ for the case of ethanol drops impacting at increasing velocities against substrates with a different roughness, reveals that the value of the critical Weber number for splashing hardly varies with ϵ namely, $We_c(\epsilon) \simeq We_c(\epsilon \simeq 0)$ if $We_\varepsilon \lesssim 1$, with $We_c(\epsilon \simeq 0)$ the critical Weber number for splashing for the case of perfectly smooth substrates, whereas We_c decreases with ϵ if $We_\varepsilon \gtrsim 1$. Thus, the experiments with ethanol depicted in figure 5 reveal that the value of the critical Weber number for splashing is only appreciably modified with respect to that found for a perfectly smooth substrate when the grit size is similar or larger than the thickness of the lamella. Let us also point out that, when $We_\varepsilon \gtrsim 1$, figure 5 also shows that, the larger We_ε is i.e. the larger surface roughness is with respect to the thickness of the thin liquid sheet, the more irregular is the shape of the ejected lamella and the larger is the angle with which drops are ejected.

However, the splashing of water drops, illustrated in figures 6 and 7 for the two types of sandpapers considered here, show that there exists a crucial difference with the analogous experiments with ethanol depicted in figure 5: $We_c(\epsilon) < We_c(\epsilon \simeq 0)$ even if $\varepsilon \ll H_t$. Indeed, figures 6 and 7 show that the critical Weber number for splashing decreases notably with respect to that of the smooth substrate even for $We_\varepsilon \ll 1$. Figure 6 shows that, similarly to the case of ethanol droplets depicted in figure 5, the value of We_c decreases with ϵ in those cases for which $We_\varepsilon \gtrsim 0.5$. Moreover, figures 6 and 7 also show that the droplet disintegrates more irregularly when ϵ increases.

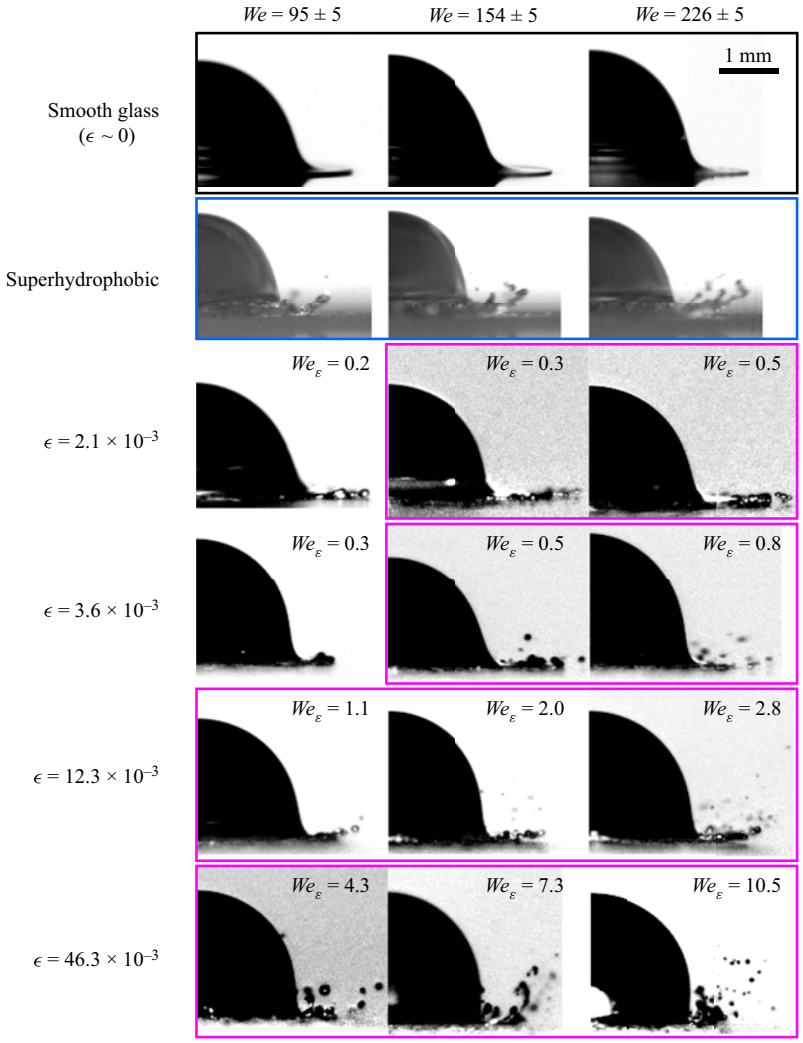

Figure 6. Experimental images showing the impact of water drops over SC sandpapers at the same dimensionless time, $t = TV/R = 0.6 \pm 0.1$ for different values of the parameters We and ϵ defined in (2.4*a–d*). The first row, highlighted in black, corresponds to the case of a smooth glass substrate, the second row, highlighted in blue, corresponds to experiments done with a SH coating (Quintero *et al.* 2019) whereas the rest of the cases correspond to SC sandpapers. The splash cases are highlighted in pink. The splash transition can also be triggered increasing ϵ for a given We.

Figure 8 illustrates the underlying reason for the differences observed in figures 5–7 between the splashing of ethanol and water droplets for the cases in which $We_\varepsilon \lesssim 1$. Indeed, it is appreciated in figure 8 that the advancing front wets the substrate for the case of ethanol and, also, that the edge of the advancing lamella is not in contact with the solid for the case of water. This different wetting behaviour is clearly not only a property of the liquid, but also of the type of substrate: notice from figure 9 that, for the case of AO substrates, the wetting behaviour of the edge of the lamella is non-monotonic for fixed values of the Weber number and increasing values of ϵ because the rim does not appear to be appreciably separated from the substrate for the particular case of $\epsilon = 0.7 \times 10^{-3}$.

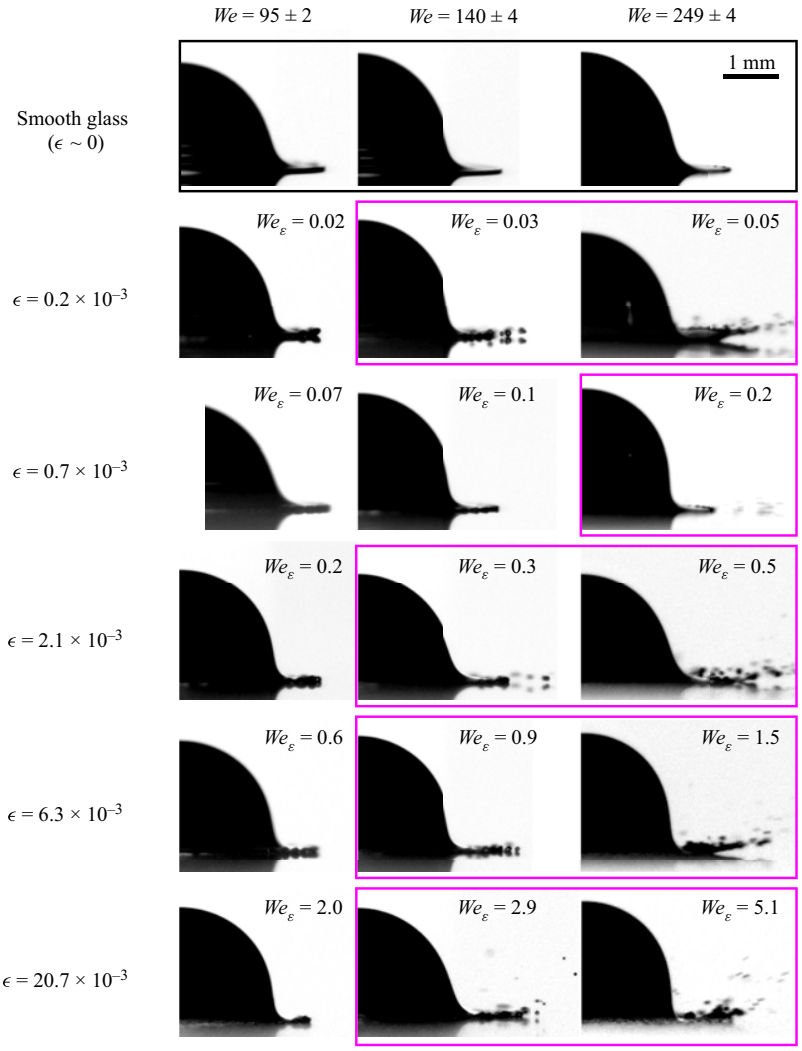

Figure 7. Experimental images showing the impact of water drops over AO sandpapers at the same dimensionless time, $t = TV/R = 0.6 \pm 0.1$ for different values of the parameters We and ϵ defined in (2.4*a–d*). The first row, highlighted in black, corresponds to the case of a smooth glass substrate, whereas the rest of cases correspond to AO sandpapers. The splash cases are highlighted in pink. The value of the critical Weber number for splashing is much larger for the case of smooth substrates.

This is the reason for the larger value of We_c for AO substrates and $\epsilon = 0.7 \times 10^{-3}$ with respect to the rest of the different substrates with different values of ϵ depicted in figures 6 and 7, for which the edge of the lamella does not wet the substrate, as figure 9 shows.

In fact, the case of ethanol droplets in figure 8, where the rim perfectly wets the substrate, resembles that found, for instance, in the first row of images in figure 6, showing the impact of a water drop against a smooth partially wetting solid, whereas the case of water in figures 8 and 9, showing that the edge of the lamella does not contact the rough solid, is qualitatively similar to the impact of a drop on a SH substrate depicted in the second row of images in figure 6.

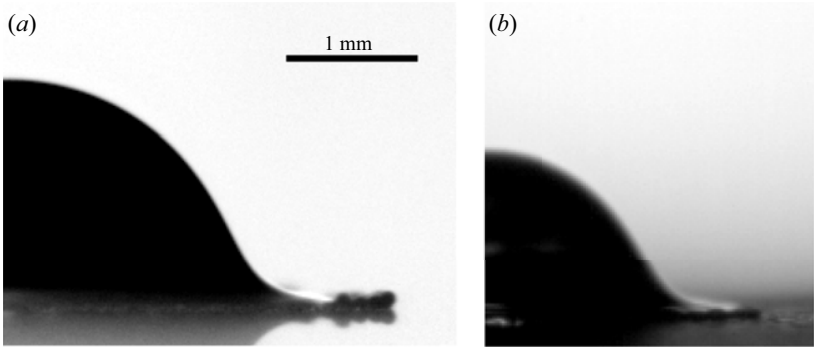

Figure 8. Experiments showing the spreading of a water drop (*a*) and of an ethanol drop (*b*) for practically the same value of the Weber number $We = 123 \pm 3$, over SC sandpapers with $\epsilon = 6.3 \times 10^{-3}$, $We_\varepsilon = 0.8$ (*a*) and $\epsilon = 8.7 \times 10^{-3}$, $We_\varepsilon = 1.1$ (*b*). Whereas it is observed that the edge of the lamella is not in contact with the solid for the case of water, the rim wets the substrate for the case of ethanol.

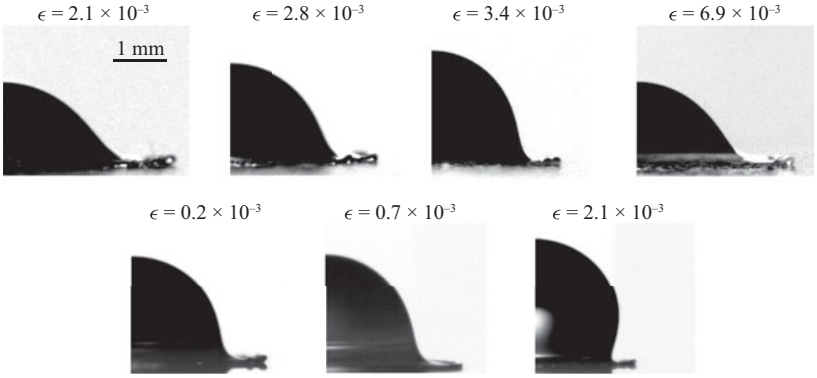

Figure 9. Experiments showing the spreading of water drops over SC substrates for $We = 80 \pm 3$ and different values of ϵ (top row) and over AO substrates for $We = 97 \pm 2$ and different values of ϵ (bottom row). In all the cases considered, $We_\varepsilon \lesssim 1$ and, except for the case corresponding to the AO sandpaper with $\epsilon = 0.7 \times 10^{-3}$, for which the critical Weber number for splashing is larger than for the rest of the values of ϵ in figure 7, the rim does not wet the substrate.

Motivated by the observations above, in the remainder of this contribution, three different theoretical frameworks will be used to predict, in an approximate way, the splash transition on rough substrates: the one for smooth partially wetting substrates deduced in Riboux & Gordillo (2014) and Gordillo & Riboux (2019) will be employed here to describe the splash transition in the case $We_\varepsilon \lesssim 1$ and the rim wets the rough substrate. Moreover, a new result will be derived to describe the splash of drops impacting on wetting substrates when $We_\varepsilon \gtrsim 1$ whereas the results in Quintero *et al.* (2019) will be used to predict the value of the critical Weber number when the rim does not wet the solid. The similitudes between the present experimental results and those previously reported for smooth or SH coatings are further supported by the experimental evidence depicted for the case of water drops in figure 10, where it is shown that, in analogy with SH substrates, air pockets are entrapped between the expanding liquid film and the solid. In contrast, figure 11 shows that, for the case of ethanol, the liquid wets the surface homogeneously, not leaving any air gaps between the lamella and the rough wall, a behaviour which is fully consistent with the additional observations in figure 12, where it is depicted that the radial position of the

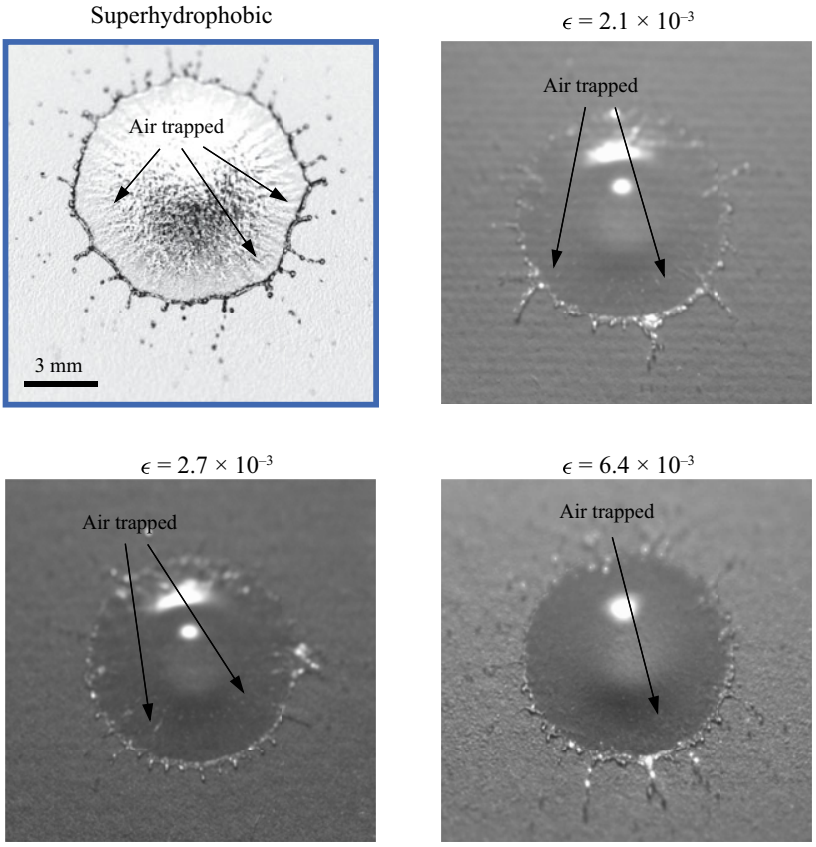

Figure 10. Air pockets are entrapped at the surface corrugations after the impact of a water drop over the SH substrate, highlighted in blue. Likewise, air bubbles are entrapped for the case of the impact of water drops over rough substrates with different values of ϵ. In all cases shown, $We = 221 \pm 4$, which is above the critical value for splashing.

rim bordering the expanding sheet increases monotonically with time, a behaviour which is already observed when drops spread over smooth partially wetting substrates. But, when the rim does not wet the substrate, as is the case of the water droplets depicted in figure 13 – see also figures 9 and 10 – the edge of the lamella retracts, this being one of the main features of the impact of drops over SH substrates (Quéré 2008).

The next section is devoted to presenting theoretical models aimed at explaining and quantifying the different experimental observations depicted in figures 5–13.

3. Theoretical models and comparison with experiments

For the case of smooth partially wetting substrates, it is shown in Riboux & Gordillo (2014) and Gordillo & Riboux (2019) that the lamella takes off from the substrate for sufficiently large values of the impact velocity because, only under these circumstances, is the vertical velocity imparted to the rim by the gas lubrication forces larger than that produced by capillary retraction. Once the lamella is no longer in contact with the substrate, the growth of capillary instabilities disintegrates the rim into droplets, giving rise to the splash of the drop (Riboux & Gordillo 2015). However, the experimental observations

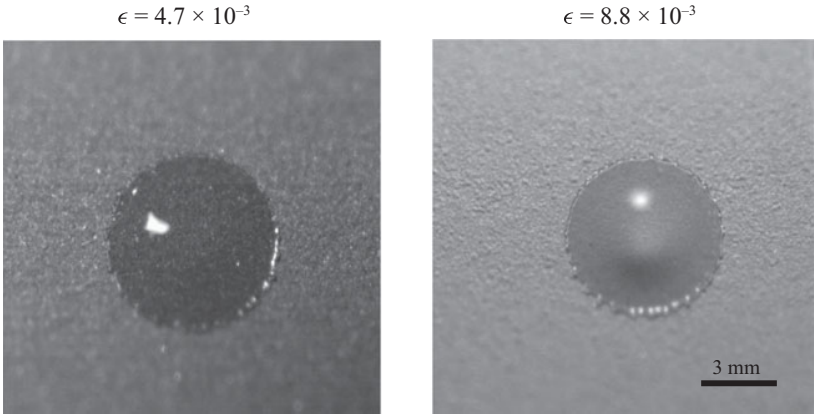

Figure 11. Air pockets are not entrapped at the surface corrugations after the impact of ethanol drops over substrates with different values of ϵ because, in this case, the liquid wets the solid. In the cases shown, $We = 216 \pm 3$, which is above the critical value for splashing.

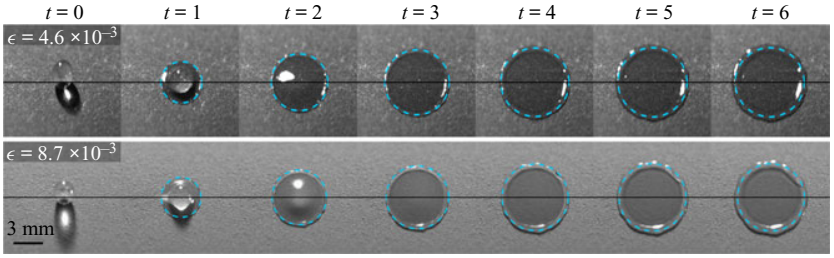

Figure 12. Spreading of ethanol drops over SC sandpapers for $We = 66 \pm 2$, a value below the critical Weber number for splashing, for the values of ϵ indicated in each of the rows. No air bubbles are entrapped between the solid and the liquid. The rim limiting the expanding liquid sheet increases monotonically with time. The blue line represents the solution of the system (3.1) in the partially wetting case, with $\gamma = 1/2$ and $\beta = 0$ and for which the rim pins the substrate at the maximum spreading radius at the short time scales of the figure. For much larger time scales the ethanol drop tends to wet the rough substrate, this capillary process not being of interest here. The horizontal line indicates the location of the drop impact point.

in Quintero *et al.* (2019) indicate that the rim is never in contact with the wall for the case of SH substrates, no matter how small the Weber number is. Thus, in the SH case, the drop will only splash when the capillary time, which is the time required for capillary instabilities to break the edge of the lamella into pieces, is smaller than the hydrodynamic time characterizing the thickening of the rim. Clearly, the splash condition differs notably depending on whether the liquid partially wets the solid or the substrate is SH.

Motivated by the experimental evidence shown in § 2, the results presented in Riboux & Gordillo (2014) and Gordillo & Riboux (2019) will be used here to characterize the splash of a drop when $We_\varepsilon \lesssim 1$ and the rim wets the substrate, whereas those results in Quintero *et al.* (2019) will be used to predict the value of the critical Weber number for splashing when the rim is not in contact with the rough substrate. The splash transition corresponding to the cases for which the liquid wets the substrate and $\varepsilon \gtrsim H_t$ i.e. when $We_\varepsilon \gtrsim 1$, will be quantified using a new theoretical approach.

However, before presenting the different theoretical frameworks used to predict the splash transition on rough substrates, we show next that the previous results in

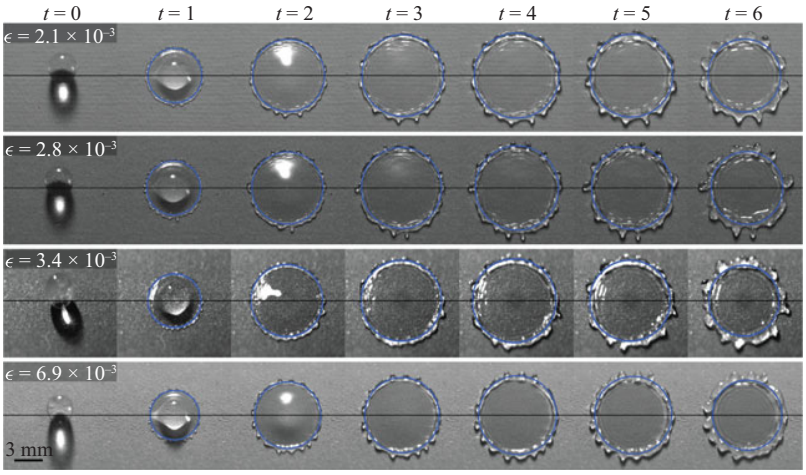

Figure 13. Spreading of water drops impacting over SC sandpapers for $We = 65 \pm 5$, a value below the critical Weber number for splashing, for the values of ϵ indicated in each of the rows. The rim limiting the expanding liquid sheet first reaches a maximum and then retracts. The blue line represents the solution of the system (3.1) in the SH limit, with $\gamma = 1$ and $\beta = 1$. Equations (3.4*a*,*b*) are used to describe the rim retraction process once the drop reaches the maximum spreading radius. The horizontal line serves to indicate the location of the impact point.

Gordillo *et al.* (2019) can be used to predict the spreading of drops on rough substrates under those experimental conditions for which $We_\varepsilon \lesssim 1$.

3.1. *Spreading of drops for* $We_\varepsilon \lesssim 1$

For drop impact velocities below those producing the splash transition, the time evolution of the rim position and thickness will be described here using the theory in Gordillo *et al.* (2019), where $t = 0$ indicates the instant the drop first contacts the solid at the so-called impact point, which is also the origin of radial distance $r = 0$. In Gordillo *et al.* (2019), the flow is divided into the following three different spatial regions, sketched in figure 14:

(i) The drop region, $0 \le r \le \sqrt{3t}$, where the liquid is accelerated by pressure gradients, with $r = \sqrt{3t}$ indicating the radius of the circular wetted area (Riboux & Gordillo 2014).

(ii) The lamella, which extends along the spatio-temporal region $\sqrt{3t} \le r \le s(t)$, is located in between the impacting drop and the rim. Since the lamella is slender, pressure gradients can be neglected.

(iii) The rim, which is located at a $r = s(t)$, possesses a thickness $b(t)$ and moves with a velocity $v(t)$. The rim refers to the edge of the expanding liquid film limiting the perimeter of the spreading drop.

The differential equations describing the time evolutions of $s(t)$, $b(t)$ and $v(t)$ are deduced from the balances of mass and momentum applied at the rim

$$\left.\begin{aligned} \gamma \frac{\pi}{4}\frac{\mathrm{d}b^2}{\mathrm{d}t} &= [u(s,t) - v]h(s,t), \quad \frac{\mathrm{d}s}{\mathrm{d}t} = v, \\ \gamma \frac{\pi b^2}{4}\frac{\mathrm{d}v}{\mathrm{d}t} &= [u(s,t) - v]^2 h(s,t) - (1+\beta)\, We^{-1}, \end{aligned}\right\} \tag{3.1}$$

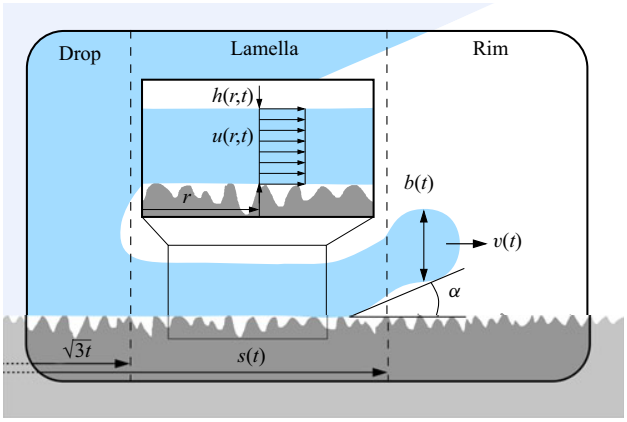

Figure 14. Sketch showing the different variables used in § 3. The flow is divided into three different parts: the drop, where pressure gradients cannot be neglected and which extends along the spatio-temporal region $0 \leq r \leq \sqrt{3t}$; the lamella, where pressure gradients can be neglected and which extends along the spatio-temporal region $\sqrt{3t} \leq r \leq s(t)$, and the rim. The rim radial position, thickness and velocity are indicated, respectively, by $s(t)$, $b(t)$ and $v(t)$ whereas $u(r, t)$ stands for the averaged radial velocity within the lamella and $h(r, t)$ represents its thickness.

with $u(r, t)$ and $h(r, t)$ indicating, respectively, the averaged radial velocity and the thickness of the lamella extending along the spatio-temporal region $\sqrt{3t} \leq r \leq s(t)$ (see figure 14). The values of the parameters γ and β in (3.1) are chosen assuming that the shape of the rim is either a circle or semicircle of diameter b and also depend on whether the rim wets or not the substrate. In the latter case, which corresponds to a SH-like behaviour, the rim is a circle and hence $\gamma = 1$ and $\beta = 1$ whereas, in the former, corresponding to a hydrophilic-like behaviour, the rim is assumed to be a semicircle and then, $\gamma = 1/2$ and $\beta = 0$. The ordinary differential equations for $s(t)$, $b(t)$ and $v(t)$ are solved particularizing at $r = s(t)$ the following analytical expressions for u and h deduced in Gordillo *et al.* (2019), valid for $Re \gg 1$:

$$\left\{\begin{aligned} u(r,t) &= \frac{r}{t} - \frac{Re^{-1/2}}{t}\left[\frac{\sqrt{3}\chi x}{2h_a(x)} + \frac{2\sqrt{3}\lambda}{7h_a(x)x^{5/2}}(t^{7/2} - x^{7/2})\right] + O(Re^{-1}), \\ h(r,t) &= 9\frac{t^2}{r^4}h_a[3(t/r)^2] + \frac{Re^{-1/2}}{rt}\left[\frac{\sqrt{3}}{2}x^2 + \frac{\sqrt{3}(105\,\chi - 60\lambda)}{42}x^3(t^{-1} - x^{-1})\right. \\ &\quad \left. + \frac{24\sqrt{3}\lambda}{105}x^{-1/2}(t^{5/2} - x^{5/2})\right] + O(Re^{-1}), \end{aligned}\right. \tag{3.2}$$

with $\lambda = 1$, $\chi = 2/3$, $x = 3(t/r)^2$ and $h_a(x)$ indicating the polynomial function also given in Gordillo *et al.* (2019). The ordinary differential equations in (3.1) are solved subjected to the following initial conditions, imposed at the dimensionless instant t_e the lamella is initially ejected (Riboux & Gordillo 2014):

$$\left.\begin{aligned} &\text{At} \quad t = t_e = 1.05\,We^{-2/3}, \quad s(t_e) = \sqrt{3t_e}, \\ &v(t_e) = \frac{\sqrt{3/t_e}}{2} \quad \text{and} \quad b(t_e) = \frac{\sqrt{12}}{\pi}t_e^{3/2}. \end{aligned}\right\} \tag{3.3}$$

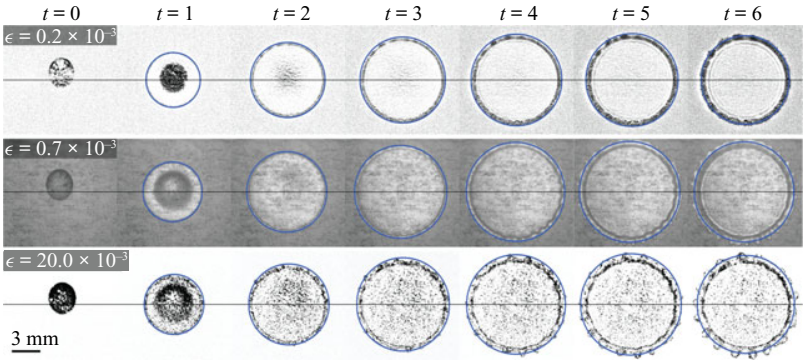

Figure 15. Spreading of water drops impacting over AO sandpapers for $We = 96 \pm 4$, a value below the critical Weber number for splashing, for the values of ϵ indicated in each of the rows. The blue line represents the solution of the system (3.1) for $\gamma = 1$ and $\beta = 1$. Equations (3.4*a*,*b*) are used to describe the rim retraction process once the drop reaches the maximum spreading radius, but only for $\epsilon = 0.2 \times 10^{-3}$ and $\epsilon = 20.0 \times 10^{-3}$ because the rim pins to the substrate once the maximum radius is reached for the case $\epsilon = 0.7 \times 10^{-3}$. The horizontal line serves to indicate the location of the impact point.

It is explained in García-Geijo *et al.* (2020) that the system of ordinary differential equations (3.1) is integrated from the ejection time $t = t_e$ up to the instant t^* for which the rim velocity vanishes namely, $v(t = t^*) = 0$, with t^* calculated solving the system (3.1). Thereafter, there exist two different possibilities depending on whether the rim wets or not the substrate: for the hydrophilic-like case, the rim pins to the solid and, thus, $s(t > t^*) = s(t = t^*)$ but, for the SH-like case, the rim retracts, namely $v(t > t^*) < 0$. The rim contraction process is described using the results in García-Geijo *et al.* (2020), where the differential equations in (3.1) are simplified by neglecting the relative fluxes of mass, $(u - v)h$, and momentum, $(u - v)^2 h$, giving the following analytical expressions for $s(t > t^*)$ and $v(t > t^*)$:

$$v = \frac{-8}{\pi b^{*2}\, We}(t - t^*) \quad \text{and} \quad s = s^* - \frac{4}{\pi\, b^{*2}\, We}(t - t^*)^2, \tag{3.4a,b}$$

with s^* and b^* the values of the rim position and thickness at the instant $t = t^*$ calculated by integrating the system (3.1). The comparison between the predictions and observations in figures 12, 13 and 15 for the two types of liquids and for the two different types of rough substrates (AO and SC) considered in this study, validate the approach presented here for arbitrary values of ϵ and $t \lesssim 10$ whenever $We_\varepsilon \lesssim 1$. Indeed, it can be appreciated from figures 5–7 that the drop disintegrates right after touching the substrate for $We_\varepsilon \gtrsim 1$ and so the description for the spreading process provided here cannot be applied when the grit size is larger than the thickness of the lamella. Let us point out here that the spreading of the drop along the substrate caused by capillarity, taking place at time scales $t \gtrsim O(10)$, is not the subject of this study.

3.2. *Splashing models for* $We_\varepsilon \lesssim 1$

Since the splashing criterion differs depending on the wetting properties of the substrate, here we consider the following two cases.

3.2.1. *Splashing model for hydrophilic-like behaviour*

It was explained in Riboux & Gordillo (2014) that the splashing of drops impacting partially wetting substrates takes place when the vertical velocity imparted to the edge of the expanding sheet is larger than the radial growth of the rim, which is caused by capillary retraction. This condition can be written as (Gordillo & Riboux 2019)

$$K_l \left(\frac{\mu_g}{\mu}\right) Oh\, We^{5/6} \simeq 0.034, \tag{3.5}$$

with μ_g the gas viscosity, We and Oh defined in (2.4*a–d*) and K_l a coefficient that accounts for the effect of the gas lubrication pressure in the wedge region formed between the substrate and the advancing liquid front, see figure 14. The value of K_l for normal atmospheric conditions is calculated using the expression given in Gordillo & Riboux (2019)

$$K_l = \frac{3}{\tan^2\alpha} \ln\left[A\left(\frac{\mu}{\mu_g}\right)^{3/4} Oh^{-1/4}\left(We\,\frac{\lambda_g}{R}\right)^{-1}\right], \tag{3.6}$$

with $\lambda_g = 68 \times 10^{-9}$ m the mean free path of gas molecules, $A = 0.011$ a constant and α the wedge angle sketched in figure 14, whose slight variations around $\alpha \sim 60^\circ$, already pointed out in Gordillo & Riboux (2019), will be later on expressed as a function of the static advancing contact angle, θ_{adv}, see table 1.

3.2.2. *Splashing model for hydrophobic-like behaviour*

It was explained in Quintero *et al.* (2019) that the splash transition for the case of SH substrates takes places when the time characterizing the radial growth of the rim, $T_h = (R/V)t_h = (R/V)(1/b\,\mathrm{d}b/\mathrm{d}t)^{-1}$, is substantially larger than the capillary time, $T_c = (R/V)t_c = (\rho R^3 b^3/8\sigma)^{1/2}$. Indeed, for capillary corrugations to be amplified up to the instant the drops are ejected from the rim, it is necessary that $t_c/t_h \lesssim 0.1$ (Riboux & Gordillo 2015), which yields the following splash criterion:

$$\frac{t_c}{t_h} = \sqrt{b/8}\frac{\mathrm{d}b}{\mathrm{d}t}\, We^{1/2} \lesssim 0.1, \tag{3.7}$$

with $b(t)$ the thickness of the rim (see figure 14) calculated through the integration of (3.1). Hence, capillary instabilities will only break the rim for values of the Weber number above a certain threshold, We_c, given by (3.7). Figure 16 illustrates how the value of We_c is determined from the solution of (3.1), (3.2) and (3.7) for $\lambda = 1$. Let us point out here that the results in figure 16 reveal that the values of the critical Weber numbers differ from those calculated in Quintero *et al.* (2019): indeed, we found a small typo in the code used to solve (3.7), which has been corrected here and which does not affect any other of the results presented in our earlier work. In fact, we have verified that the experimental values for the splash threshold velocity corresponding to SH substrates measured in Quintero *et al.* (2019) are very well predicted by the solution of (3.7) with smaller values of λ ($\lambda < 1$) in (3.1) and (3.2), a fact indicating that, as expected, the more slippery is the non-wetting substrate, the smaller is the value of the friction factor λ.

Notice that (3.7) describes the spreading to splashing transition in cases of drops with $Oh \ll 1$ impacting over non-wetting dry substrates at normal atmospheric conditions. Indeed, the gas pockets entrapped at the corrugations, which are responsible for the SH-like behaviour depicted in figures 6 and 7, could not be present for small values of the ambient pressure.

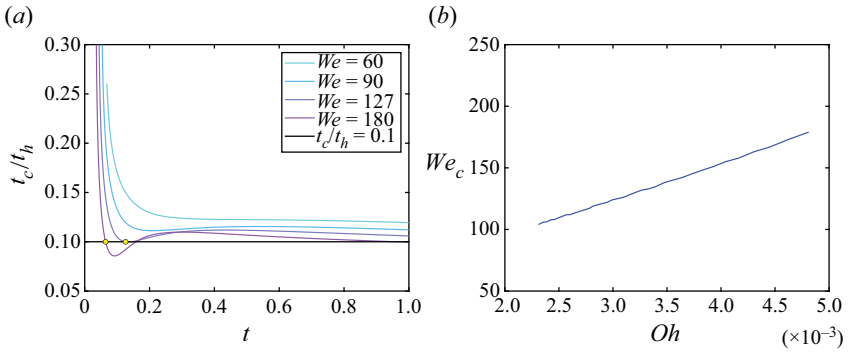

Figure 16. (*a*) Time evolution of the ratio t_c/t_h defined in (3.7) calculated solving (3.1) and (3.2) for $\gamma = 1$, $\beta = 1$, $\lambda = 1$ and different values of the Weber number for $Oh = 3.1 \times 10^{-3}$. Notice that the ratio t_c/t_h is below the threshold value 0.1 only for values of the Weber number $We \gtrsim 125$. (*b*) Dependence of the value of the critical Weber number, We_c on Oh for $\lambda = 1$.

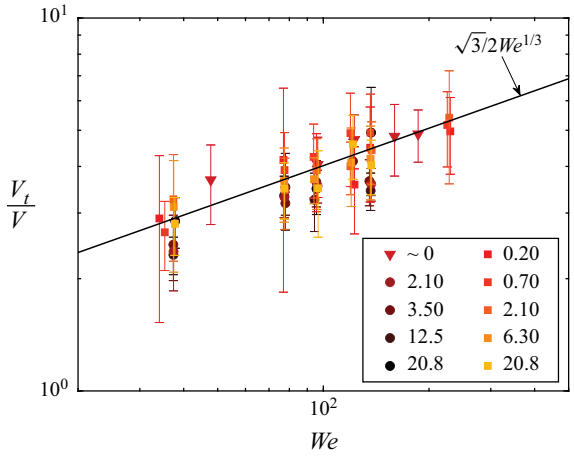

Figure 17. The measured velocity at which the lamella is initially ejected is in good agreement with the predicted value, $V_t/V \simeq \sqrt{3}/2\, We^{1/3}$, given in (2.5*a*,*b*), for the AO and SC substrates in table 1. The values accompanying each of the symbols in the legend – a triangle for glass, circles for SC sandpapers and squares for AO sandpapers – indicate $10^3 \times \epsilon$.

3.3. *Splashing criterion for wetting substrates and* $We_\varepsilon \gtrsim 1$

The experimental evidence shown in figures 5–7 reveals that, for the cases in which the grit size is such that $\varepsilon > H_t$ or, equivalently $We_\varepsilon \gtrsim 1$, a lamella is not formed and the drop disintegrates producing roughly cylindrical fingers which break as a consequence of the growth of capillary instabilities. Then, for the drop to splash in this regime, it is first necessary that a jet with a typical diameter $\sim \varepsilon$ is formed, which implies that the liquid velocity $V_t = (\sqrt{3}/2)V\, We^{1/3}$ at the instant when it is ejected along the substrate protuberances, is larger than the Taylor–Culick velocity

$$V_{TC} \propto \sqrt{\sigma/(\rho\varepsilon)}, \tag{3.8}$$

with the exact prefactor in (3.8) given in e.g. Hoepffner & Paré (2013). Figure 17 shows that, indeed, the lamella is ejected at the velocity predicted by (2.5*a*,*b*) and, in spite of

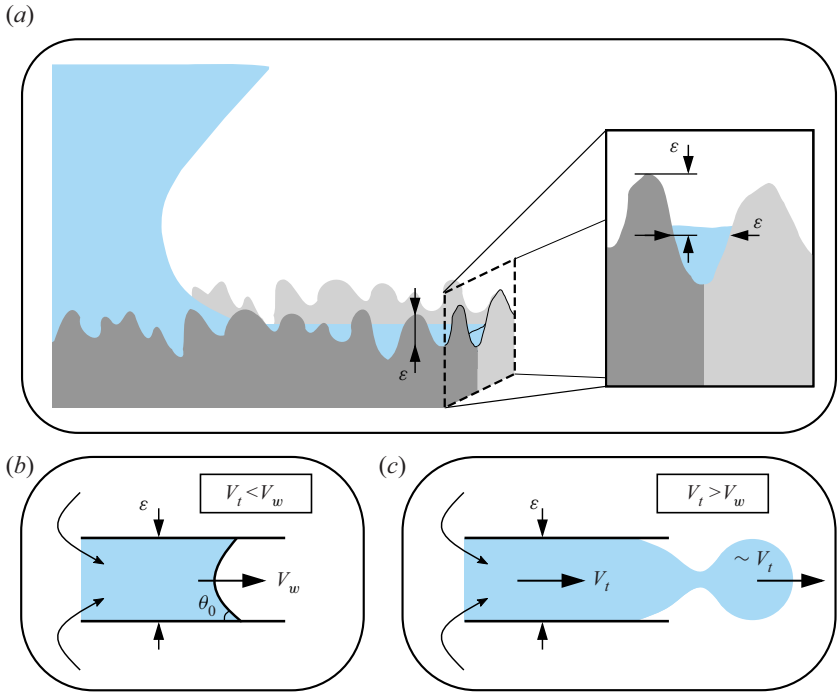

Figure 18. (*a*) Sketch illustrating one of the main ideas behind the model developed to predict the splash transition for $We_\varepsilon \gtrsim 1$: we assume that the liquid flows along channels of characteristic width ε and that splashing occurs when the velocity V_t – see figure 17 – of a jet with a characteristic thickness $\sim \varepsilon$ is larger than both the Taylor–Culick velocity (3.8) and the wetting velocity V_w given in (3.9). Here, both the Taylor–Culick velocity and the wetting velocity given in (3.9) are calculated with the simplifying hypothesis that the liquid flows along cylinders with a diameter ε, and so similar ideas to those in Quéré (1997) can be used to calculate V_w. Panel (*b*) illustrates that no splash will occur if the liquid velocity V_t – see figure 17 – is smaller than the wetting velocity, $V_t < V_w$. Panel (*c*) illustrates a case in which splash occurs because the liquid velocity V_t is larger than the wetting velocity, $V_t > V_w$.

the fact that we could not record experimental images with sufficiently good spatial and temporal resolutions so as to measure the dependence of the thickness of the ligaments with the substrate roughness, our qualitative measurements in the Appendix and the results in Xu *et al.* (2007) indicate that the width of the ejected fingers depends on ε. However, (3.8) is not the only restriction for a ligament to be formed: it is also necessary that V_t is faster than the velocity V_w with which the liquid wets the interstices formed over the rough substrate, see the sketch in figure 18(*a*). Indeed, in this way, the height of the liquid film along the 'channels' of width ε increases in time until it is larger than the grit size ε, producing the ejection of a liquid thread above the corrugated substrate, which acts as a ramp if, in addition, $V_t > V_{TC}$. Since, for the low viscosity liquids considered here, the Ohnesorge number based on ε is such that $Oh_\varepsilon = Oh\epsilon^{-1/2} \ll 1$ for $We_\varepsilon \gtrsim 1$, the wetting velocity V_w can be calculated assuming the simplifying hypothesis that the liquid flows along a cylinder of diameter ε – see figure 18 – as

$$\frac{1}{2}\rho V_w^2 \sim \frac{4\sigma\cos\theta_0}{\varepsilon} \Rightarrow V_w \sim \sqrt{8\cos\theta_0}V_{TC}, \tag{3.9}$$

with V_{TC} given in (3.8) and θ_0 the Young contact angle, which slightly differs from the experimental value of θ, see (2.3) and table 1. Notice that the balance expressed by (3.9)

between the dynamic pressure and the capillary pressure beneath a spherical meniscus forming an angle θ_0 with the walls of a circular channel of diameter ε, is proportional to that reported by Quéré (1997) in his analysis of the initial instants of the capillary rise of low viscosity liquids in cylindrical tubes. It is expected that (3.9) holds if

$$\frac{\sqrt{\nu T_c}}{\varepsilon} = \frac{\sqrt{\nu\varepsilon/V_t}}{\varepsilon} = Re^{-1/2}We^{-1/6}\epsilon^{-1/2} \ll 1 \Rightarrow We^{-5/12}Oh^{1/2}\epsilon^{-1/2} \ll 1, \quad (3.10)$$

namely, if the width of the boundary layer developed during the characteristic residence time $T_c \sim \varepsilon/V_t = \varepsilon/VWe^{-1/3}$ is much smaller than the width of the channel $\sim \varepsilon$, a condition which is clearly verified here because $We \gg 1$ and $Oh \ll 1$. Notice that the same type of balance as that expressed by (3.9) between inertia and capillary pressure, holds during coalescence of two drops of radii R (Biance, Clanet & Quéré 2004; Winkels *et al.* 2012) or when a drop wets a wall, a process which was found by Bird, Mandre & Stone (2008) to be influenced by the value of the static contact angle but not by the viscous dissipation at the advancing contact line.

In view of the discussion above, it is expected that the drop will splash when the most restrictive of the conditions

$$\frac{V_t}{V_{TC}} \gtrsim 1 \Rightarrow We \gtrsim \epsilon^{-3/5} \quad \text{and} \quad \frac{V_t}{V_w} \gtrsim 1 \Rightarrow We \gtrsim K_w(8\cos\theta_0)^{3/5}\epsilon^{-3/5}, \quad (3.11a,b)$$

with K_w an order-unity constant to be determined from experiments, is satisfied. The reason for the constant K_w in (3.11*a*,*b*) is that (3.9) rests on the assumption that the geometry of the rough substrate can be viewed as that of a cylinder of diameter ε. It is expected that the clear differences existing between the real geometry and that of a cylinder can be accounted for through the adjustable constant K_w.

The values of We_c calculated using the theoretical approximations explained above are compared with our own experimental data in figure 19, whereas the comparisons between experiments and the correlations proposed by Range & Feuillebois (1998) and Tang *et al.* (2017), are provided in the Appendix. The experimental data in Range & Feuillebois (1998), corresponding to values of $Oh \simeq 3 \times 10^{-3}$, are also included in figure 19. Since the prediction in (3.11*a*,*b*) does not depend on Oh, those experimental data for which $We_\varepsilon \gtrsim 1$ in Hao (2017), Tang *et al.* (2017), as well as those corresponding to the normal impact of drops on rough substrates in Aboud *et al.* (2020), have also been included in figure 19. Notice that our description is limited to $\epsilon < 0.1$ since, for larger values of the substrate roughness the separation of scales between the grit size ε and the drop radius R is small and the splash transition will depend on the local geometry of the substrate around the impact point.

For those cases in which the rim wets the substrate and $We_\varepsilon \lesssim 1$, the values of the critical Weber number for splashing have been calculated using the results in Gordillo & Riboux (2019), where it was pointed out that the wedge angle $\alpha \approx 60^\circ$ in (3.5) slightly depends on the wetting properties of the surface, with larger values of α for smaller values of the contact angle. This fact justifies the following empirical equation for α:

$$\alpha = 62.5^\circ - 9^\circ[\theta_{adv}/90^\circ], \quad (3.12)$$

where the value of $\alpha(\theta_{adv} = 0) = 62.5^\circ \approx 60^\circ$ corresponding to liquids such as ethanol, methanol or acetone was already reported in Riboux & Gordillo (2014) and the small prefactor $9^\circ/90^\circ = 0.1$ has been chosen in order to maximize the agreement between experimental measurements and predictions.

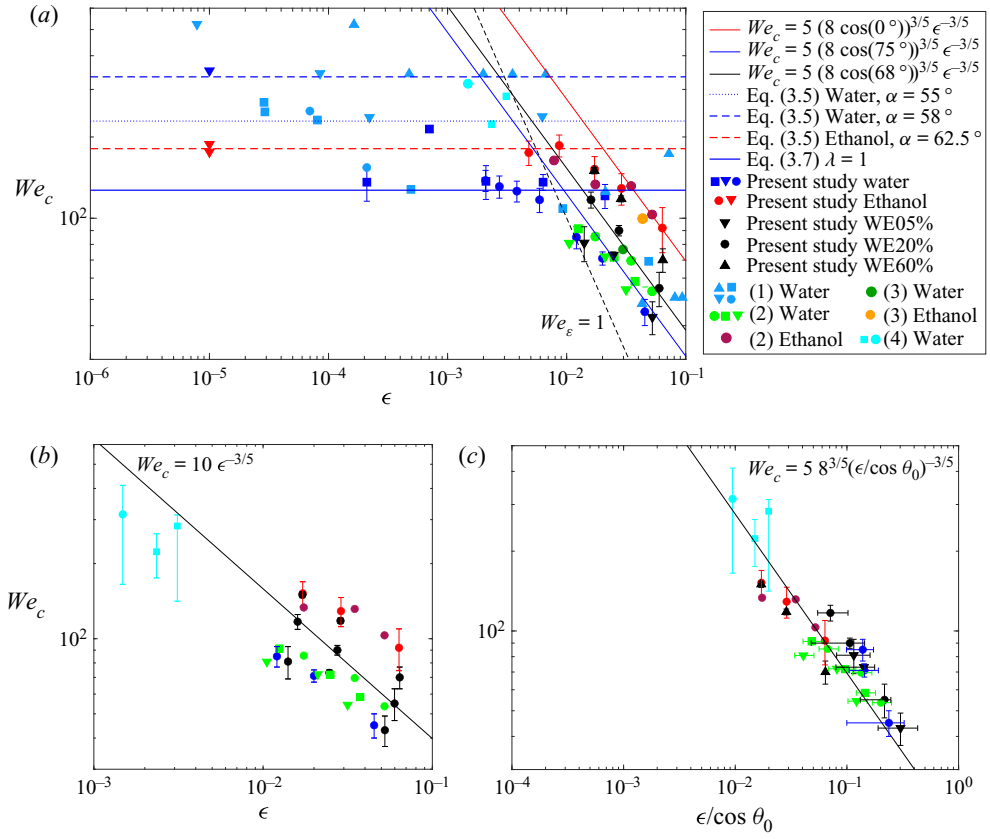

Figure 19. (*a*) For the case of wetting substrates and $We_\varepsilon \lesssim 1$, the values of the critical Weber number have been calculated using (3.5) and (3.12) with $Oh = 7.3 \times 10^{-3}$ (ethanol) and $Oh = 3.1 \times 10^{-3}$ (water) whereas, for the case of water drops and non-wetting substrates, the value of the critical Weber number has been calculated using (3.7) with $t_c/t_h = 0.1$, $\lambda = 1$ and $Oh = 3.1 \times 10^{-3}$. The values of We_c for $We_\varepsilon \gtrsim 1$ have been calculated using the second equation in (3.11*a*,*b*) with the value of the free constant adjusted to $K_w = 5$ and using the values of the Young contact angle θ_0 given in table 2. The experimental data points in Range & Feuillebois (1998), Tang *et al.* (2017) and Aboud, Wood & Kietzig (2020) have been included in the figure once (2.1) has been used to express R_a as a function of ε. Here, [1] Range & Feuillebois (1998), [2] Hao (2017) and [3] Tang *et al.* (2017); the experimental data in [4] Aboud *et al.* (2020) for $We_\varepsilon \gtrsim 0.5$ are also included here because figures 6 and 7 show that the rough-induced transition to splashing for the case of water takes place for values of We_ε slightly smaller than 1. The values of θ_{adv}, needed to calculate the value of α in (3.5), (3.6) and (3.12), are provided in either the original references or in tables 1 and 2. The experimental values of the critical Weber number for splashing, corresponding to the condition $We_\varepsilon \gtrsim 1$, have been represented in (*b*) as a function of ϵ and in (*c*) as a function of $\epsilon/\cos\theta_0$. Panel (*c*) shows that the experimental data follow the prediction in (3.11*a*,*b*), $We_c \propto (\epsilon/\cos\theta_0)^{-3/5}$. The black symbols in (*a*–*c*) indicate additional experiments carried out here using mixtures of water and ethanol for different values of the ethanol mass fraction (in %). The material properties of the mixtures as well as the corresponding values of the contact angles are indicated in table 2. The acronym WE followed by a number indicates the proportion of ethanol in the water–ethanol mixture.

The splash velocities predicted by (3.5) and (3.12) using the measured values of θ_{adv} given in tables 1 and 2 are compared with the experimental values corresponding to either rough or smooth substrates with different wettabilities and different liquids in figures 19 and 20(*a*), validating our approach. Interestingly, (3.5) and (3.12) predict that the splash

Surface	Liquid	θ	θ_0	θ_{adv}
P220 SC SP	Water	$45 \pm 18^\circ$	$71 \pm 8^\circ$	—
P220 SC SP	WE 05 %	$55 \pm 10^\circ$	$79 \pm 5^\circ$	—
P220 SC SP	WE 20 %	$33 \pm 3^\circ$	$70 \pm 7^\circ$	—
P220 SC SP	WE 60 %	$3 \pm 1^\circ$	SHydrophilic $\sim 0^\circ$	—
P220 SC SP	Ethanol	$\sim 0^\circ$	SHydrophilic $\sim 0^\circ$	—
P500 SC SP	Water	$65 \pm 3^\circ$	$82 \pm 3^\circ$	—
P500 SC SP	WE 05 %	$50 \pm 12^\circ$	$77 \pm 5^\circ$	—
P500 SC SP	WE 20 %	$36 \pm 12^\circ$	$67 \pm 12^\circ$	—
P500 SC SP	WE 60 %	$2 \pm 1^\circ$	SHydrophilic $\sim 0^\circ$	—
P500 SC SP	Ethanol	$\sim 0^\circ$	SHydrophilic $\sim 0^\circ$	—
P1000 SC SP	Water	$74 \pm 1^\circ$	$85 \pm 2^\circ$	—
P1000 SC SP	WE 05 %	$68 \pm 5^\circ$	$83 \pm 3^\circ$	—
P1000 SC SP	WE 20 %	$52 \pm 7^\circ$	$77 \pm 4^\circ$	—
P1000 SC SP	WE 60 %	$3 \pm 1^\circ$	SHydrophilic $\sim 0^\circ$	—
P1000 SC SP	Ethanol	$\sim 0^\circ$	SHydrophilic $\sim 0^\circ$	—
SC SP	Water	—	$75 \pm 12^\circ$	—
SC SP	WE 05 %	—	$78 \pm 7^\circ$	—
SC SP	WE 20 %	—	$68 \pm 13^\circ$	—
SC SP	WE 60 %	—	$\sim 0^\circ$	—
SC SP	Ethanol	—	$\sim 0^\circ$	—
Smooth Glass	Water	—	—	32°
Rough Glass (P4000)	Water	—	—	49°
Rough Glass (P500)	Water	—	—	20°
Parafilm	Water	—	—	109°
Smooth PlexiGlass	Water	—	—	76°
Rough PlexiGlass (P4000)	Water	—	—	89°
Rough PlexiGlass (P500)	Water	—	—	146°
Smooth Glass	Ethanol	—	—	$\sim 0^\circ$
Smooth Glass	Methanol	—	—	$\sim 0^\circ$
Smooth Glass	Acetone	—	—	$\sim 0^\circ$
Smooth Glass	Decamethyltetrasiloxane	—	—	$\sim 0^\circ$
Smooth Glass	Dodecamethylpentasiloxane	—	—	$\sim 0^\circ$
Smooth Glass	Isopropanol	—	—	$\sim 0^\circ$
Smooth Glass	1:4 (v/v) Glycerol/water	—	—	32°
Stainless Steel	Water	—	—	84°
Stainless Steel	Ethanol	—	—	$\sim 0^\circ$

Table 2. Values of the contact angle θ, of the Young contact angle θ_0 and of the advancing contact angle θ_{adv} for drops of different liquids over different types of substrates. The values of θ_0 have been calculated using the measured values of θ taking $f = 3$ in figure 3. With the purpose of comparing our predictions with the measured splash velocities reported by Range & Feuillebois (1998), Tang *et al.* (2017) and Hao (2017), the values of the advancing contact angles for stainless steel, glass and Plexiglas substrates, which can be either smooth or roughened using the type of sandpaper indicated in parenthesis, are also given in the table. The values of the static advancing contact angle for the liquids used in Riboux & Gordillo (2014) and Palacios *et al.* (2013) are also provided here. The material properties corresponding to the different water–ethanol (WE) mixtures used here and characterized by the ethanol mass fraction, are the following (de Goede *et al.* 2021): (i) 5 % of ethanol, $\rho = 989.0$ kg m^{-3}, $\sigma = 56.4$ mN m^{-1}, $\mu = 1.23 \times 10^{-3}$ Pa s, (ii) 20 % of ethanol: $\rho = 968.7$ kg m^{-3}, $\sigma = 38.0$ mN m^{-1}, $\mu = 2.14 \times 10^{-3}$ Pa s, (iii) 60 % of ethanol, $\rho = 891.1$ kg m^{-3}, $\sigma = 26.2$ mN m^{-1}, $\mu = 2.55 \times 10^{-3}$ Pa s.

threshold velocity decreases when θ_{adv} increases. A similar result was very recently reported by Quetzeri-Santiago *et al.* (2019*a*,*b*) who, however, quantified the effect of the substrate wettability on the splash transition by modifying the value of the parameter

β in Riboux & Gordillo (2014) and Gordillo & Riboux (2019). Therefore, the results in figure 20(a) contrast with those in Range & Feuillebois (1998) for the case of drops impacting over smooth Plexiglas substrates and also with those in de Goede *et al.* (2018) for the case of drops of water–ethanol mixtures impacting over smooth parafilm substrates. Indeed, Range & Feuillebois (1998) and de Goede *et al.* (2018) find that the splash threshold velocity is mostly independent of the substrate wettability whereas the results in (3.5) and (3.12) and figures 19 and 20(a) reveal that larger values of θ_{adv} favour the splash transition. The reason for the discrepancies found with previous results lies on the fact that the disintegration process for the case of water drops takes place at very small time and length scales, which are only observable using the adequate spatial and temporal resolutions, as it is shown in figures 20(c)–20(d).

Figures 19 and 20(b) also confirm that the solution of (3.1), (3.2) and (3.7) with $\lambda = 1$ can be used to predict the value of the critical Weber number for the case of non-wetting rough substrates.

But, possibly, the most interesting result shown in figure 19 is that the second of the equations in (3.11a,b), which depends on the static contact angle but which does not depend on the Ohnesorge number provided that $Oh\,\epsilon^{-1/2} \ll 1$, can be used to predict the splash transition when the liquid wets the substrate and $We_\varepsilon \gtrsim 1$ namely, when the thickness of the lamella is similar or smaller than the grit size. The results obtained here for $We_\varepsilon \gtrsim 1$ have been confirmed in a separate and independent study by de Goede *et al.* (2021) for different liquids and values of Oh. Notice that figure 19 also includes the experimental results corresponding to different water–ethanol mixtures, with values of the Young angle θ_0 given in table 2. The good agreement between the calculated and the measured splash velocities provide further support to the second of the equations in (3.11a,b), which can then be used to predict the value of We_c when the liquid wets the substrate and $We_\varepsilon \gtrsim 1$.

Let us point out that the comparison between predictions and experiments in figure 19 reveals that the value of the critical Weber number corresponding to the case of AO sandpaper with $\epsilon = 0.7 \times 10^{-3}$ is well above our predicted value for non-wetting substrates. The reason for this particular behaviour was already pointed out above and it is clearly depicted in figures 7 and 9: the rim is not clearly separated from the solid in this case. But, what is the reason this specific sandpaper behaves so differently with respect to the rest of the cases investigated? To answer this question, let us turn back to the findings in Roisman *et al.* (2015), where it was suggested that droplet splashing is not controlled by the height of the substrate roughness but by a parameter measuring the slope of the corrugations: in fact, this is not the case because the results in figure 19 for $We_\varepsilon > 1$ confirm the essential role played by the height and width of the corrugations in triggering the splashing of droplets. However, the observation made by Roisman *et al.* (2015), together with the results depicted in figure 19, suggest that the splashing of droplets on rough substrates when $\theta < 90^\circ$ depends on ϵ and also on the dimensionless parameter measuring the slope of the corrugations defined in (2.2). Indeed, the values of S_{dq} in table 1 reveal that the value of the slope of the corrugations for the case of the lime AO sandpaper with $\epsilon = 0.7 \times 10^{-3}$ is far smaller than for the rest of the cases, with a value of the static contact angle $\theta < 90^\circ$. Then, for a given value of ϵ, two different values for the splash velocity are possible depending on whether the advancing rim wets the substrate, which happens for $S_{dq} \lesssim 1$, or not. This dual behaviour of the rough substrate, which manifests itself through two different values of We_c for the same value of ϵ, can be clearly seen in figure 19 for $We_\varepsilon \lesssim 1$. As a final remark, please recall that the results presented here have been deduced for the case in which neither the spatial distribution nor the geometry of

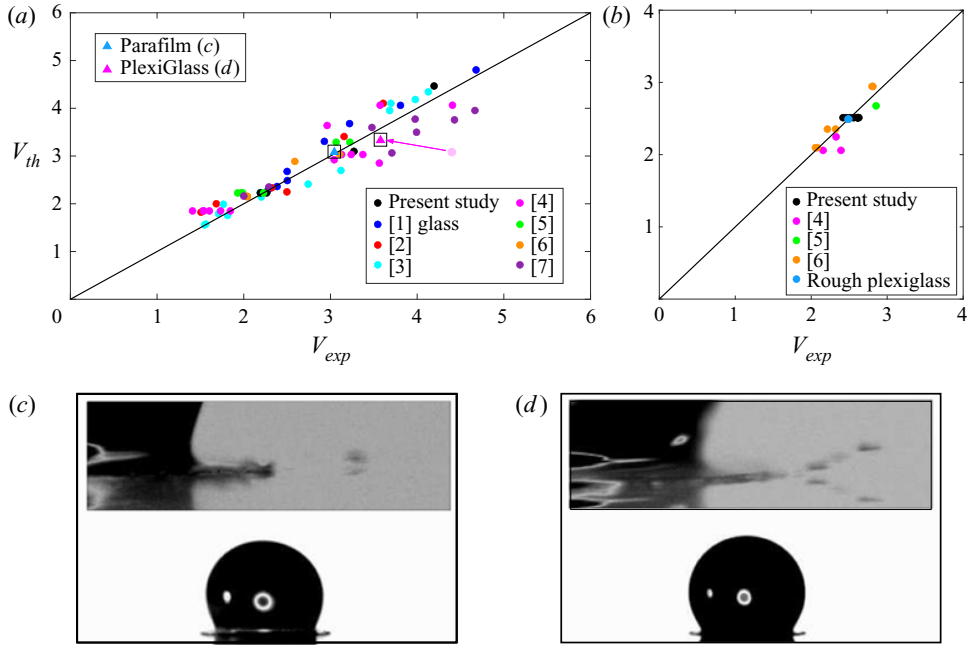

Figure 20. (*a*) Analysis of the cases for which the liquid wets the substrate and $We_\varepsilon < 1$: comparison between the measured splash velocity V_{exp} and the calculated value V_{th} using (3.5) and (3.12), $\alpha = 62.5^\circ - 9^\circ[\theta_{adv}/90^\circ]$ with θ_{adv} given in tables 1 and 2 or in the original references. A total of 68 experimental data points for different liquids, drop sizes and values of the Ohnesorge number varying within the range $2.3 \times 10^{-3} < Oh < 1.87 \times 10^{-2}$ are represented in this figure. Experiments taken from the present experimental study and from [1] de Goede *et al.* (2021) for the case of glass substrates, [2] Palacios *et al.* (2013), [3] Riboux & Gordillo (2014), [4] Range & Feuillebois (1998), [5] Tang *et al.* (2017), [6] Hao (2017), [7] Aboud *et al.* (2020). This figure also contains the experimental data corresponding to the case of water drops with $Oh = 3.1 \times 10^{-3}$ falling over parafilm and Plexiglas substrates depicted in (*c*,*d*). The splash velocities for the squared blue triangle, which corresponds to the case of parafilm and the pink triangle corresponding to the case of smooth Plexiglas, located at the left of the light pink circle representing the original data in Range & Feuillebois (1998), are smaller than for the case of glass substrates. The reason for this behaviour is that the values of θ_{adv} for parafilm and Plexiglas are larger than for the case of smooth glass substrates (see table 2) and, in agreement with the predictions in (3.5) and (3.12), the values of the splash threshold velocities are smaller than the one corresponding to the case of a smooth glass substrate. (*b*) Comparison between the measured splash velocity V_{exp} and the value V_{th} calculated from (3.1), (3.2) and (3.7) with $\lambda = 1$ for the case of water drops impacting over SH substrates. This figure displays a total of 20 experimental data points, including the experiments in figure 19, the additional experiments corresponding to roughened Plexiglas substrates also obtained here as well as those in [4] Range & Feuillebois (1998), [5] Tang *et al.* (2017), [6] Hao (2017). The value of the Ohnesorge number varies within the range $2.65 \times 10^{-3} < Oh < 3.5 \times 10^{-3}$. Panels (*c*,*d*), which show the impact of water drops with $Oh = 3.1 \times 10^{-3}$ over parafilm (*c*) and Plexiglas (*d*), illustrate the importance of the spatial and the temporal resolution in order to correctly measure the splash velocity. The main images in (*c*,*d*) have been recorded at 13 333 f.p.s. and possess a spatial resolution of $\sim$30 μm pixel^{-1}, whereas the insets have been recorded at 156 321 f.p.s. with a spatial resolution of $\sim$5.5 μm pixel^{-1}. Whereas no splash is observed in the main images with lower spatial and temporal resolutions, the insets show that the main drop does in fact disintegrate into smaller pieces.

the protuberances is controlled: the extrapolation of the present results to those cases of microfabricated substrates in which the height, width, spacing and shape of the pillars are varied independently should be the subject of a separate study.

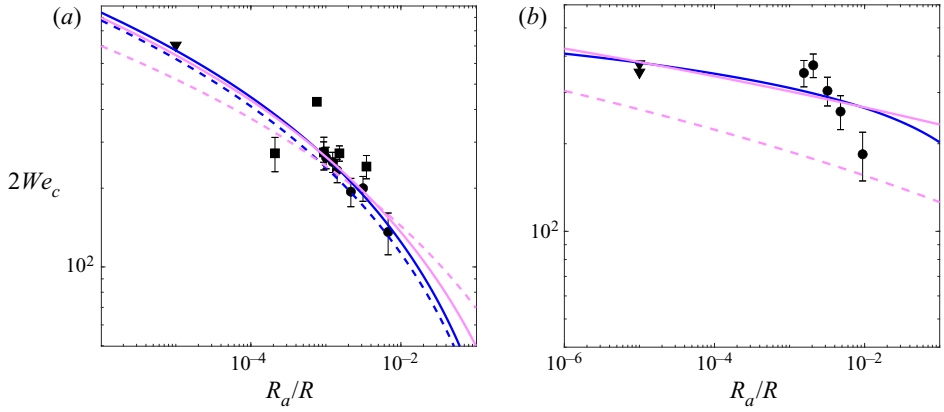

Figure 21. Comparison between our experimental data – black symbols – for the cases of water (*a*) and ethanol (*b*) with the correlations proposed by Range & Feuillebois (1998) and Tang *et al.* (2017), see table 3. The meaning of the different types of lines depicted in these plots is indicated in table 3: dashed lines are used to represent the correlations using the original values of the free constants whereas the continuous lines are used to represent the predictions using the values of the constants that best fit to our data. Blue/pink lines are used to plot the correlations proposed by Range & Feuillebois (1998) and Tang *et al.* (2017), respectively.

4. Conclusions

In this contribution we report experimental results obtained when millimetric drops of water and ethanol of radii R fall over sandpapers with different values of the substrate roughness, ε. The analysis of the high-speed videos recorded reveals that the spreading or splashing of the impacting drops crucially depends on the value of the ratio between the height of the corrugations and the initial thickness of the lamella, a dimensionless parameter which can be expressed as $We_\varepsilon = \rho V^2 \varepsilon/\sigma$ using the theory in Riboux & Gordillo (2014). It is shown here that, when $We_\varepsilon \lesssim 1$ and the impact velocity is below the splash threshold, the spreading of the drop over the surface can be described using the theory in Gordillo *et al.* (2019) and, in addition, that the transition from spreading to splashing crucially depends on the wetting properties of the substrate. Indeed, when the advancing rim wets the solid, the splash transition can be predicted using the results for smooth solids in Gordillo & Riboux (2019) when the slight variations of the wedge angle around $\alpha \sim 60^\circ$ are expressed as a function of the static advancing contact angle. However, if the rim does not wet the substrate, the value of the critical Weber number for splashing, We_c, can be calculated using the theoretical framework presented in Quintero *et al.* (2019) for the case of SH substrates. When the liquid wets the substrate and $We_\varepsilon \gtrsim 1$, it is also shown here that the splash threshold velocity decreases with ε as $We_c \propto (R\cos\theta_0/\varepsilon)^{3/5}$, with θ_0 the Young contact angle.

Acknowledgements. This work has been supported by the Spanish MINECO under Project DPI2017-88201-C3-1-R, partly financed through European funds.

Declaration of interests. The authors report no conflict of interest.

Author ORCIDs.
P. García-Geijo http://orcid.org/0000-0001-8608-4804;
G. Riboux https://orcid.org/0000-0003-2395-1653;
J. M. Gordillo http://orcid.org/0000-0003-1431-3780.

	Range & Feuillebois (1998)		Tang *et al.* (2017)	
Type of surface	Aluminium, glass, Plexiglass		Stainless steel	
Values of $\frac{R_a}{R}$	$8.0 \times 10^{-6} - 2.2 \times 10^{-2}$		$2.6 \times 10^{-5} - 6.7 \times 10^{-3}$	
Correlation	$We_c' = a \ln^b \left(\frac{R}{R_a}\right)$		$\left(\frac{We_c'}{Oh'}\right)^{\frac{1}{2}} = a + b \ln\left(\frac{R_a}{2R}\right)$	
Liquid	Water	Ethanol	Water	Ethanol
Values of original fitting constants	$a = 6.47$ $b = 1.87$	— —	$a = 77.8$ $b = -33.7$	$a = 133.6$ $b = -7.5$
Type of line				
Values of adjusted fitting constants	$a = 7.74$ $b = 1.84$	$a = 145.86$ $b = 0.39$	$a = 23.48$ $b = -42.64$	$a = 192.78$ $b = -6.49$
Type of line				

Table 3. Correlations provided by Range & Feuillebois (1998) and Tang *et al.* (2017). The values of the fitting constants for water and ethanol are either those given by the authors, or those found by a least-square fitting to our own data. Notice that Range & Feuillebois (1998) and Tang *et al.* (2017) define *We* and *Oh* using the diameter of the droplet and so $We_c' = 2\,We_c$ and $Oh' = 1/\sqrt{2}\,Oh$.

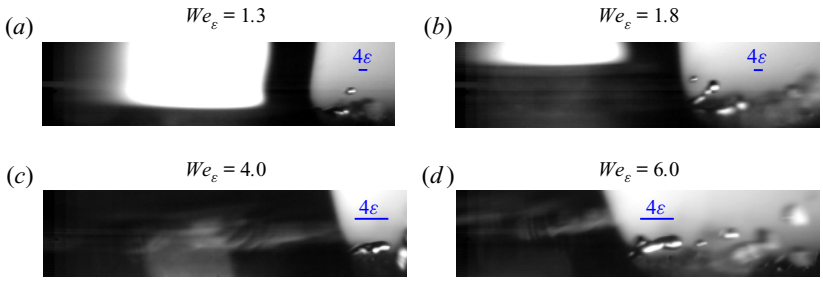

Figure 22. First row: experimental images corresponding to the SC P1000 sandpaper, with $\varepsilon = 18$ μm, recorded at 100 000 f.p.s. with a spatial resolution of 5.7 μm pixel^{-1}. The images shown correspond to the instant $t = T\,V/R = 0.4 \pm 0.05$. Second row: experimental images corresponding to the SC P220 sandpaper, with $\varepsilon = 68$ μm, recorded at 60 000 f.p.s. with a spatial resolution of 5.7 μm pixel^{-1}. The images shown correspond to the instant $t = T\,V/R = 0.6 \pm 0.06$. The values of We_ε are indicated at each of the images and the scale bar in each of the images represents 4ε.

Appendix

Here, we compare our experimental measurements with the correlations provided by Range & Feuillebois (1998) and Tang *et al.* (2017). The results obtained are shown in figure 21, see also table 3. Figure 22 qualitatively shows the dependence with ε of the diameters of the ligaments and of the drops ejected when $We_\varepsilon \gtrsim 1$.

References

Aboud, D.G.K., Wood, M.J. & Kietzig, A.-M. 2020 Influence of liquid properties on the oblique splashing threshold of drops. *Phys. Fluids* **32** (6), 061402.

Almohammadi, H. & Amirfazli, A. 2017 Understanding the drop impact on moving hydrophilic and hydrophobic surfaces. *Soft Matter* **13**, 2040–2053.

BIANCE, A.-L., CLANET, C. & QUÉRÉ, D. 2004 First steps in the spreading of a liquid droplet. *Phys. Rev.* E **69**, 016301.
BIRD, J.C., MANDRE, S. & STONE, H.A. 2008 Short-time dynamics of partial wetting. *Phys. Rev. Lett.* **100**, 234501.
BIRD, J.C., TSAI, S.S.H. & STONE, H.A. 2009 Inclined to splash: triggering and inhibiting a splash with tangential velocity. *New J. Phys.* **11**, 063017.
BURZYNSKI, D.A., ROISMAN, I.V. & BANSMER, S.E. 2020 On the splashing of high-speed drops impacting a dry surface. *J. Fluid Mech.* **892**, A2.
CIMPEANU, R. & MOORE, M.R. 2018 Early-time jet formation in liquid-liquid impact problems: theory and simulations. *J. Fluid Mech.* **856**, 764–796.
EXTRAND, C.W. & KUMAGAI, Y. 1995 Liquid drops on an inclined plane: the relation between contact angles, drop shape, and retentive force. *J. Colloid Interface Sci.* **170** (2), 515–521.
GADELMAWLA, E.S., KOURA, M.M., MAKSOUD, T.M.A., ELEWA, I.M. & SOLIMAN, H.H. 2002 Roughness parameters. *J. Mater. Process. Technol.* **123** (1), 133–145.
GARCÍA-GEIJO, P., RIBOUX, G. & GORDILLO, J.M. 2020 Inclined impact of drops. *J. Fluid Mech.* **897**, A12.
DE GOEDE, T., DE BRUIN, K., SHAHIDZADEH, N. & BONN, D. 2021 Droplet splashing on rough surfaces. *Accepted for publication in Phys. Rev. Fluids*.
DE GOEDE, T.C., LAAN, N., DE BRUIN, K.G. & BONN, D. 2018 Effect of wetting on drop splashing of newtonian fluids and blood. *Langmuir* **34** (18), 5163–5168.
GORDILLO, J.M. & RIBOUX, G. 2019 A note on the aerodynamic splashing of droplets. *J. Fluid Mech.* **871**, R3.
GORDILLO, J.M., RIBOUX, G. & QUINTERO, E.S. 2019 A theory on the spreading of impacting droplets. *J. Fluid Mech.* **866**, 298–315.
HAO, J. 2017 Effect of surface roughness on droplet splashing. *Phys. Fluids* **29**, 122105.
HAO, J. & GREEN, S.I. 2017 Splash threshold of a droplet impacting a moving substrate. *Phys. Fluids* **29**, 012103.
HAO, J., LU, J., LEE, L., WU, Z., HU, G. & FLORYAN, J.M. 2019 Droplet splashing on an inclined surface. *Phys. Rev. Lett.* **122**, 054501.
HOEPFFNER, J. & PARÉ, G. 2013 Recoil of a liquid filament: escape from pinch-off through creation of a vortex ring. *J. Fluid Mech.* **734**, 183–197.
DE JONG, R., ENRÍQUEZ, O.R. & VAN DER MEER, D. 2015 Exploring droplet impact near a millimetre-sized hole: comparing a closed pit with an open-ended pore. *J. Fluid Mech.* **772**, 427–444.
JOSSERAND, C., LEMOYNE, L., TROEGER, R. & ZALESKI, S. 2005 Droplet impact on a dry surface: triggering the splash with a small obstacle. *J. Fluid Mech.* **524**, 47–56.
JOSSERAND, C. & THORODDSEN, S.T. 2016 Drop impact on a solid surface. *Annu. Rev. Fluid Mech.* **48**, 365–391.
JOSSERAND, C. & ZALESKI, S. 2003 Droplet splashing on a thin liquid film. *Phys. Fluids* **15**, 1650–1657.
KIM, H., PARK, U., LEE, C., KIM, H., HWAN KIM, M. & KIM, J. 2014 Drop splashing on a rough surface: how surface morphology affects splashing threshold. *Appl. Phys. Lett.* **104** (16), 161608.
LATKA, A., STRANDBURG-PESHKIN, A., DRISCOLL, M.M., STEVENS, C.S. & NAGEL, S.R. 2012 Creation of prompt and thin-sheet splashing by varying surface roughness or increasing air pressure. *Phys. Rev. Lett.* **109**, 054501.
LEMBACH, A.N., TAN, H. -B., ROISMAN, I.V., GAMBARYAN-ROISMAN, T., ZHANG, Y., TROPEA, C. & YARIN, A.L. 2010 Drop impact, spreading, splashing, and penetration into electrospun nanofiber mats. *Langmuir* **26** (12), 9516–9523.
MUNDO, C., SOMMERFELD, M. & TROPEA, C. 1995 Droplet-wall collisions: experimental studies of the deformation and breakup process. *Intl J. Multiphase Flow* **21**, 151–173.
ONDA, T., SHIBUICHI, S., SATOH, N. & TSUJII, K. 1996 Super-water-repellent fractal surfaces. *Langmuir* **12** (9), 2125–2127.
PALACIOS, J., HERNANDEZ, J., GOMEZ, P., ZANZI, C. & LOPEZ, J. 2013 Experimental study of splashing patterns and the splashing/deposition threshold in drop impacts onto dry smooth solid surfaces. *Exp. Therm. Fluid Sci.* **44**, 571–582.
QUÉRÉ, D. 1997 Inertial capillarity. *Europhys. Lett.* **39** (5), 533–538.
QUÉRÉ, D. 2008 Wetting and roughness. *Annu. Rev. Mater. Res.* **38** (1), 71–99.
QUETZERI-SANTIAGO, M.A., CASTREJÓN-PITA, A.A. & CASTREJÓN-PITA, J.R. 2019*a* The effect of surface roughness on the contact line and splashing dynamics of impacting droplets. *Sci. Rep.* **9** (1), 1–10.
QUETZERI-SANTIAGO, M.A., YOKOI, K., CASTREJÓN-PITA, A.A. & CASTREJÓN-PITA, J.R. 2019*b* Role of the dynamic contact angle on splashing. *Phys. Rev. Lett.* **122**, 228001.

QUINTERO, E.S., RIBOUX, G. & GORDILLO, J.M. 2019 Splashing of droplets impacting superhydrophobic substrates. *J. Fluid Mech.* **870**, 175–188.

RANGE, K. & FEUILLEBOIS, F. 1998 Influence of surface roughness on liquid drop impact. *J. Colloid Interface Sci.* **203**, 16–30.

RIBOUX, G. & GORDILLO, J.M. 2014 Experiments of drops impacting a smooth solid surface: a model of the critical impact speed for drop splashing. *Phys. Rev. Lett.* **113**, 024507.

RIBOUX, G. & GORDILLO, J.M. 2015 The diameters and velocities of the droplets ejected after splashing. *J. Fluid Mech.* **772**, 630–648.

RIOBOO, R., TROPEA, C. & MARENGO, M. 2001 Outcomes from a drop impact on solid surfaces. *Atomiz. Sprays* **11** (2), 155–165.

ROISMAN, I.V., LEMBACH, A. & TROPEA, C. 2015 Drop splashing induced by target roughness and porosity: the size plays no role. *Adv. Colloid Interface Sci.* **222**, 615–621.

SHIBUICHI, S., ONDA, T., SATOH, N. & TSUJII, K. 1996 Super water-repellent surfaces resulting from fractal structure. *J. Phys. Chem.* **100** (50), 19512–19517.

STEVENS, C.S. 2014 Scaling of the splash threshold for low-viscosity fluids. *Europhys. Lett.* **106**, 24001.

STOW, C.D., HADFIELD, M.G. & ZIMAN, J.M. 1981 An experimental investigation of fluid flow resulting from the impact of a water drop with an unyielding dry surface. *Proc. R. Soc. Lond.* A **373**, 419–441.

TANG, C., QIN, M., WENG, X., ZHANG, X., ZHANG, P., LI, J. & HUANG, Z. 2017 Dynamics of droplet impact on solid surface with different roughness. *Intl J. Multiphase Flow* **96**, 56–69.

TSAI, P., VAN DER VEEN, R., VAN DE RAA, M. & LOHSE, D. 2010 How micropatterns and air pressure affect splashing on surfaces. *Langmuir* **26** (20), 16090–16095.

WINKELS, K.G., WEIJS, J.H., EDDI, A. & SNOEIJER, J.H. 2012 Initial spreading of low-viscosity drops on partially wetting surfaces. *Phys. Rev.* E **85**, 055301.

XU, L. 2007 Liquid drop splashing on smooth, rough, and textured surfaces. *Phys. Rev. E* **75**, 056316.

XU, L., BARCOS, L. & NAGEL, S.R. 2007 Splashing of liquids: interplay of surface roughness with surrounding gas. *Phys. Rev.* E **76**, 066311.

XU, L., ZHANG, W.W. & NAGEL, S.R. 2005 Drop splashing on a dry smooth surface. *Phys. Rev. Lett.* **94**, 184505.

YARIN, A.L. 2006 Drop impact dynamics: splashing, spreading, receding, bouncing.... *Annu. Rev. Fluid Mech.* **38**, 159–192.

YARIN, A.L., ROISMAN, I.V. & TROPEA, C. 2017 *Collision Phenomena in Liquids and Solids*. Cambridge University Press.

4 Role of liquid viscosity and of air entrapped on the splashing of drops impacting over superhydrophobic substrates

Here we analyze the splash transition of drops of liquids with different viscosities impacting normally over different types of rough superhydrophobic substrates, finding that the velocity for the splash transition, V^*, increases for increasing values of the liquid viscosity and also when the proportion of air entrapped at the substrate corrugations decreases. Our experimental results also reveal that the amount of air entrapped between the drop and the wall increases with the value of the relative roughness ε/R, with ε and R indicating the amplitude of the corrugations and the radius of the drop, respectively. We show that our experimental values of V^*, as well as those reported in similar contributions in the literature, can be predicted using the splashing model presented by Quintero, Riboux & Gordillo [42], once the liquid shear stress at the wall is expressed as a decreasing function of λ, namely, of the proportion of air entrapped at the substrate.

En este capítulo se analiza la transición al *splash* de gotas de líquidos con diferente viscosidad al impactar perpendicularmente sobre distintos tipos de sustratos superhidrófobos. En el estudio experimental se observa que la velocidad crítica de *splash*, V^*, aumenta tanto para mayores valores de la viscosidad del líquido así como cuando la proporción de aire atrapado en las irregularidades del sustrato disminuye. De hecho, los resultados experimentales muestran que la cantidad de aire atrapado entre la gota y el sustrato aumenta con el valor de la rugosidad relativa ε/R, siendo ε y R la amplitud de las irregularidades y el radio de la gota respectivamente. En este capítulo se demuestra que tanto los valores experimentales de V^* obtenidos en nuestro estudio así como otros presentados en otras contribuciones de la literatura, se pueden predecir usando el modelo

de *splash* propuesto por Quintero, Riboux & Gordillo [42] una vez que los esfuerzos cortantes del flujo en la pared son expresados como una función decreciente del factor de fricción λ o, lo que es lo mismo, de la proporción de aire atrapado en el sustrato.

Paper reference:

García-Geijo, P., Riboux, G., & Gordillo, J. (2022). Role of liquid viscosity and of air entrapped on the splashing of drops impacting over superhydrophobic substrates. *Physical Review Fluids*, **7**, 093606. doi:10.1103/PhysRevFluids.7.093606

Physical Review Fluids:
Impact Factor: 2.895 (JCR 2021)
Category: Physics, Fluids & Plasmas
Category Rank: 14/34 (JCR 2021)
Category Quartile: Q2 (JCR 2021)

Scan the QR code for accessing paper in the publisher website:

5 Conclusions

When a drop impacts a solid substrate it will either spread tangentally to the surface or, if the impact velocity is large enough, it will splash disintegrating into tiny droplets which are ejected radially outwards. In this thesis we have extended the ideas in previous works [16, 37, 38, 42] and we have also presented new theoretical and experimental results in order to account for the influence of substrate inclination, wettability and roughness on the processes of spreading or in the transition from spreading to splashing under normal atmospheric conditions. Our main contributions in this thesis can be summarized as it is detailed below.

5.1 Spreading

In contrast with the case of normal drop impact, the time evolving shapes developed when a drop impacts on inclined surfaces are asymmetric since the drop elongates in a preferential direction as it expands over the surface. The spreading of a drop on an inclined substrate has been described here by including the influence of the angle of inclination χ in the theoretical model previously reported by Ref. [16] where the drop expansion process when the liquid impacts normally to a solid wall is addressed. The angle formed between the impact direction and the normal vector to the substrate possesses a clear effect on the boundary layer flow, which is not axisymmetric as in the normal impact case. Yet, the greatest effect of the inclination angle on the drop spreading proccess relies on the pinning of the advancing contact line over the solid, which does not take place simultaneously for the different angular positions along the drop perimeter. Indeed, this effect is the main reason explaining the asymmetries observed during drop spreading on an inclined substrate.

Thus, the asymmetries observed when a drop impacts over solids with different inclination angles is solved by applying balances of mass and momentum at the rim based on the ideas reported in Ref. [16]. The resulting theory provides analytical expressions that accurately predict the experimental results for the temporal evolution of the drop asymmetric shape from the instant when the drop touches the solid until the moment

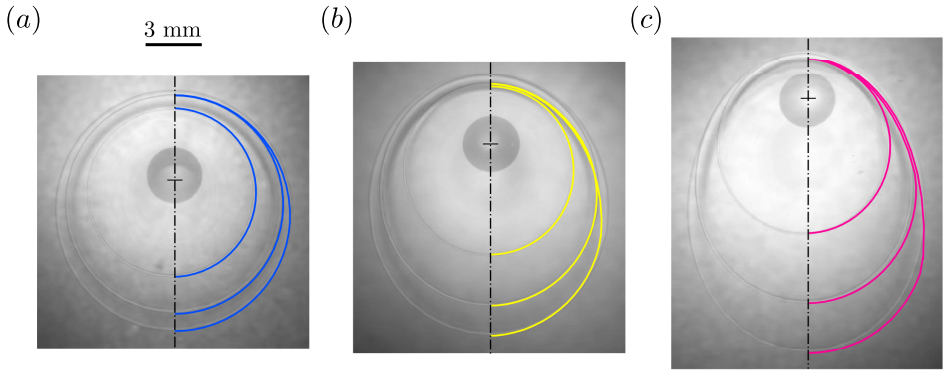

Figura 5.1 Superimposed experimental images of the water drop spreading shapes at different instants of time: $t = TV/R = 0, 2, 4$ and 6, impacting at approximately the same value of Weber number, $We = \rho(V\cos\chi)^2 R/\sigma = 120 \pm 4$, onto inclined glass slides that form an angle (a) $\chi = 15^\circ$, (b) $\chi = 30^\circ$ and (c) $\chi = 45^\circ$ with the horizontal. The solid coloured lines correspond to the solution of the proposed spreading model (see Chapter 2). The impact point is indicated with a cross.

when the rim sticks to the surface, $t \sim 6$ (see figure 5.1). At this point, the rim remains static and the drop attains its final shape. Indeed, the liquid stain that remains on the wall, possesses a shape that can be approximated to that of an ellipse whose major and minor semiaxes can be predicted using the algebraic equations deduced in Chapter 2. Through these simple expressions, which are obtained by further simplifying the above mentioned spreading model, we are able to reproduce fairly well the final shape of the drop (see figure 5.2). Moreover, these equations are still valid even at larger dimensionless times, of the order $t \sim 10^3$, for which gravitational effects can no longer be neglected: in fact, our algebraic equations reproduce fairly well the contour of the stain exceptuating the long draining rivulet which develops at the bottom part of the drop as a consequence of gravity. These results are of great interest for applications related with ink-jet printing, where the maximum expansion radius of the drop needs to be determined as a function of the control parameters. Furthermore, substantial information, such as the drop impact velocity or the impact direction, can be inferred from the analysis of the final shape of the drop thanks to our closed algebraic expressions, which therefore possess potential applications in forensic sciences.

5.2 Splashing

When the impact velocity is large enough, the drop disintegrates into smaller pieces (droplets) which are ejected radially outwards from the impacting region. As it was pointed out in the introduction, the critical velocity for splashing depends on the substrate roughness and wettability, with these surface properties being related with each other. Figure 5.3

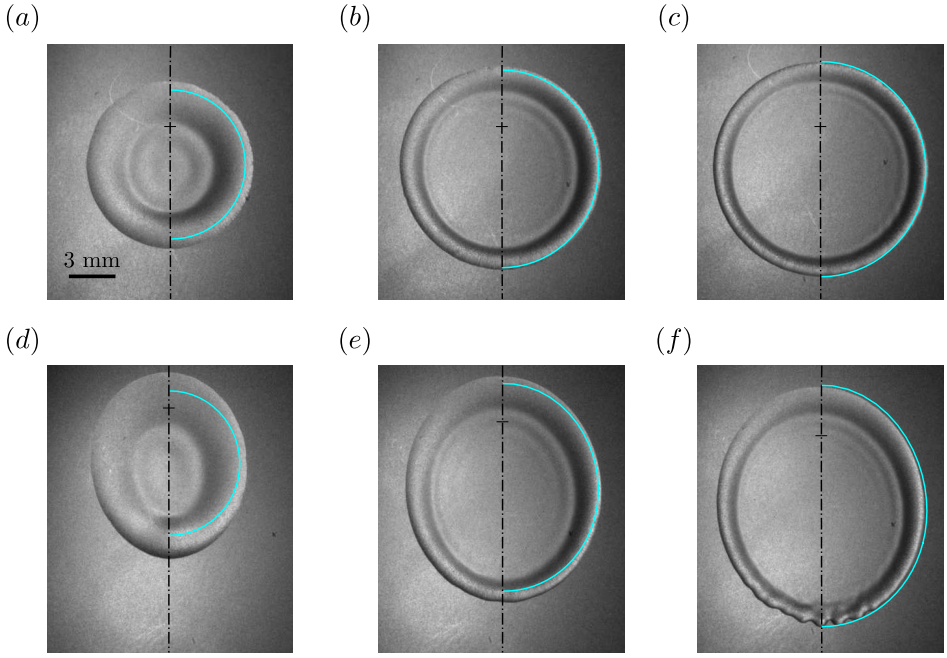

Figura 5.2 Experimental images corresponding to the stain left by a water drop impacting on a surface with two different values of the inclination angle for different values of the Weber number, $We = \rho(V\cos\chi)^2 R/\sigma$: (a) $\chi = 15^\circ$ $We = 36$, (b) $\chi = 15^\circ$ $We = 103$, (c) $\chi = 15^\circ$ $We = 163$, (d) $\chi = 30^\circ$ $We = 29$, (e) $\chi = 30^\circ$ $We = 82$, and (f) $\chi = 30^\circ$ $We = 132$. Blue lines correspond to the solution of the algebraic equations deduced in order to determine the final shape of the drop after spreading (see Chapter 2). All the experimental images correspond to approximately the same instant of time, $t = TV/R = 10 \pm 0.09$, when the rim is already pinned to the surface and the final drop shape has been attained. The impacting point is indicated with a cross.

summarizes the main contributions in this thesis since it characterizes, for a given value of the Ohnesorge number, the different types of splashing depending on two parameters, namely, the substrate wettability, measured through the value of the static contact angle θ_0, and also the relative substrate roughness, ε/R. Notice that, for the case of hydrophobic substrates, $\theta_0 > \pi/2$, the splash transition depends on the friction factor λ, which is a function of the amount of air entrapped between the liquid and the substrate and, hence, it is a function of the amplitude of the surface corrugations, as it is detailed in Chaper 4.

5.2.1 Hydrophilic splashing

The case of partially wetting substrates, when $\theta_0 < \pi/2$ which corresponds to the pink region in figure 5.3, can in turn be divided in two different regimes depending on the

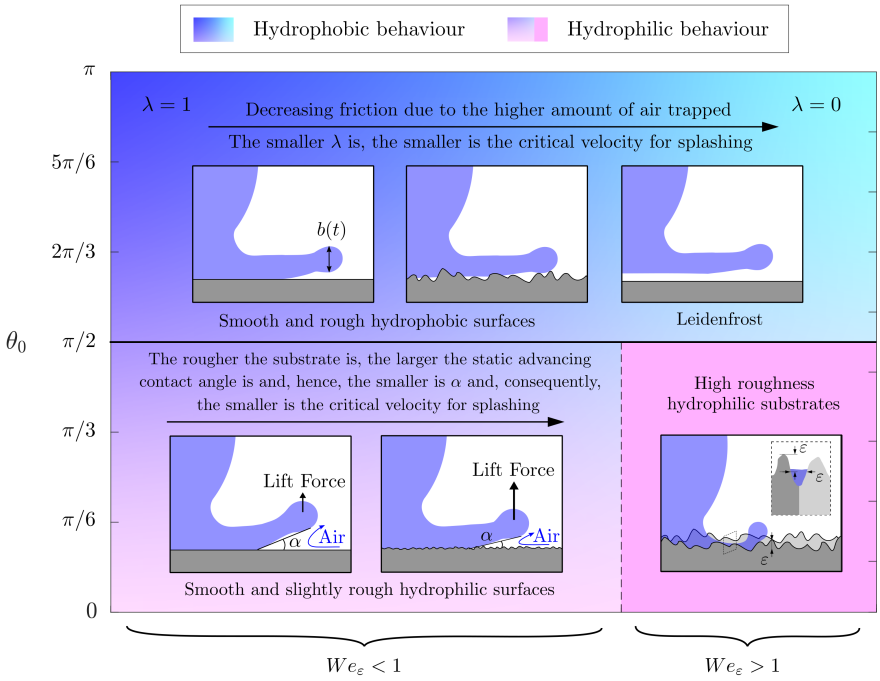

Figura 5.3 Drop splashing at normal atmospheric conditions can be classified in three main regimes: for the case of hydrophilic substrates, the critical conditions for splashing depends on the value of the parameter $We_\varepsilon = \rho V^2 \varepsilon/\sigma$. If $We_\varepsilon < 1$ and $\theta_0 < \pi/2$, the edge of the expanding lamella needs to lift off from the surface first for splashing to occur and, hence, the spreading-splashing transition can be predicted using the theory in Refs. [37, 38] which corresponds to the cases of smooth partially wetting substrates once the new equation for $\alpha = \alpha(\theta_{adv})$ proposed here (see Chapter 4) is employed. But, if the solid is hydrophilic and $We_\varepsilon > 1$, drop splashing occurs when the liquid velocity in the lamella is larger than the velocity at which the liquid wets the corrugations. For the case of hydrophobic substrates, $\theta_0 > \pi/2$, the rim does not contact the substrate and the splash criterion changes to the one deduced in Ref. [42], which depends on the time evolution of the thickness of the rim that borders the expanding lamella. This thickness depends on the friction between the liquid and the solid through the dimensionless friction factor λ [16], whose value decreases as the amount of air entrapped between the drop and substrate increases, as it is detailed in Chapter 4.

value of the parameter $We_\varepsilon = \rho V^2 \varepsilon/\sigma$ firstly identified here and which expresses the ratio between the height of the corrugations, ε, and the thickness of the ejected lamella (see Chapter 3).

When $We_\varepsilon \lesssim 1$, drop splashing is limited by the condition put forward in [37] for the case of smooth hydrophilic surfaces once the influence of the static advancing contact angle, θ_{adv}, is taken into consideration in the value of the wedge angle α, see Figure 5.3. This splashing criterion is based on the idea that the rim needs to be separated first from the substrate with a vertical velocity that needs to be larger than the velocity of radial growth of the rim caused by capillary retraction. The vertical velocity needed for the rim to lift off from the wall is induced by the air lubrication force at the wedge region of angle α developed between the advancing lamella and the solid: indeed this aerodynamic force is proportional to the product of the relative velocity between the rim and the surrounding atmosphere and $1/\tan^2\alpha$, being α a function of the static advancing contact angle, which increases with the substrate rugosity. Indeed, as it was pointed out in Ref. [38], $\alpha \sim 60^\circ$ and its value slightly varies with wetting properties of the surface, with larger values of α and, hence, smaller values of the lift force, for smaller values of θ_{adv}. Let us emphasize here that the proposed empirical equation for α as a decreasing function of the static advancing contact angle presented here for the first time (see Chapter 3) together with the term $1/\tan^2\alpha$, explains why the critical velocity for splashing in corrugated substrates is smaller than for the case of smooth substrates when $\theta_0 < \pi/2$ and $We_\varepsilon \lesssim 1$.

However, when the amplitude of the hydrophilic substrate corrugations is larger than the thickness of the lamella namely, $We_\varepsilon \gtrsim 1$, the previous splash criterion is no longer valid because the width of the lamella is similar or even smaller than the height of the surface asperities. Indeed, under these conditions, a lamella is not developed, but the liquid flows along channels of characteristic width ε (see figure 5.3). Thus, splashing takes place when a jet of typical diameter ε is formed and the speed at which this jet is ejected, is larger than the velocity at which the liquid wets the channels formed by the corrugations of width ε.

5.2.2 Hydrophobic splashing

Finally, for the case of drops impacting superrepelent surfaces, $\theta_0 > \pi/2$, which corresponds to the blue region in figure 5.3, it is observed that the advancing rim is never in contact with the substrate, regardless of the substrate roughness. Based on this observation, Ref. [42] proposed a model to predict the splash transition for the case of superhydrophobic surfaces which notably differs from the criteria presented for hydrophilic substrates because, in this case, drop splashing is limited by the growth rate of the rim thickness. Indeed, as it was discussed at length in Ref. [45], the edge bordering the expanding lamella disintegrates into tiny droplets only if capillary disturbances grow faster than the rim thickness $b(t)$ (see figure 5.3). Experiments also reveal that the value of the critical Weber number for splashing, We^*, decreases as the wall shear stress is reduced. Indeed, an increase of either the friction factor, λ, or of the Ohnesorge number, yields to larger values of We^*. Moreover, the amount of air pockets present between the impacting drop and the wall clearly increases with the amplitude of the substrate asperities. Therefore, when surface roughness is higher, the value of the friction factor decreases because of the larger proportion of air entrapped in the corrugations. Motivated by these facts, λ

is expressed in this thesis just as a decreasing function of ε through an empirical linear piecewise relationship (see Chapter 4), thus extending the previous results reported in Refs. [42, 45].

5.3 Concluding remarks

In conclusion, the spreading-splashing transition can be accurately predicted making use of the equations deduced in this thesis, which extend the previous results in Refs. [16, 37, 38, 42, 45] by explicitly including in the resulting expressions the influence of both the static contact angle and of the substrate roughness. The theoretical models put forward in this thesis compare favourably with the experimental measurements corresponding to liquids of different viscosities impacting over substrates with varying wettabilities and rugosities.

5.4 Outlook

Future work should focus on analysing the spreading of liquids with higher viscosities over inclined substrates and also the effect of viscosity and roughness on the splash transition when the drop impacts obliquely over the wall. Finally, it will be of particular interest to physically understand the drop impact process when the surface is prewetted by a liquid film with a known and controllable thickness.

Bibliografía

[1] L. da Vinci. *Codex Leicester (Codex Hammer).* 1508–1510.

[2] E. Villermaux and B. Bossa. Drop fragmentation on impact. *J. Fluid Mech.*, 668:412–435, 2011.

[3] A. M. Worthington. On the forms assumed by drops of liquids falling vertically on a horizontal plate. *Proc. R. Soc. Lond.*, 25:261–272, 1877.

[4] A. M. Worthington. A second paper on the forms assumed by drops of liquids falling vertically on a horizontal plate. *Proc. R. Soc. Lond.*, 25:498–503, 1877.

[5] C. D. Adam. Fundamental studies of bloodstain formation and characteristics. *Forensic Science International*, 219(1):76 – 87, 2012.

[6] S. Brodbeck. Introduction to bloodstain pattern analysis. *Journal for Police Science and Practice*, 2:51–57, 2012.

[7] N. Laan, K. G. de Bruin, D. Slenter, J. Wilhelm, M. Jermy, and D. Bonn. Bloodstain pattern analysis: implementation of a fluid dynamic model for position determination of victims. *Sci. Rep.*, 5:11461, 2015.

[8] C. Josserand and S. T. Thoroddsen. Drop impact on a solid surface. *Annu. Rev. Fluid Mech.*, 48:365–391, 2016.

[9] T. Gilet and L. Bourouiba. Fluid fragmentation shapes rain-induced foliar disease transmission. *J. R. Soc. Interface*, 12:20141092, 2018.

[10] S. Lejeune, T. Gilet, and L. Bourouiba. Edge effect: Liquid sheet and droplets formed by drop impact close to an edge. *Phys. Rev. Fluids*, 3:083601, Aug 2018.

[11] A.L. Yarin. Drop impact dynamics: Splashing, spreading, receding, bouncing. . . *Ann. Rev. Fluid Mech.*, 38:159–192, 2006.

[12] R. Rioboo, C. Tropea, and M. Marengo. Outcomes from a drop impact on solid surfaces. *Atomization and Sprays*, 11(2), 2001.

[13] L. Xu, L. Barcos, and S. R. Nagel. Splashing of liquids: Interplay of surface roughness with surrounding gas. *Phys. Rev. E.*, 76:066311, 2007.

[14] A. Latka, A. Strandburg-Peshkin, M.M. Driscoll, C.S. Stevens, and S.R. Nagel. Creation of prompt and thin-sheet splashing by varying surface roughness or increasing air pressure. *Phys. Rev. Lett.*, 109:054501, 2012.

[15] J. Hao. Effect of surface roughness on droplet splashing. *Physics of Fluids*, 29:122105, 2017.

[16] J. M. Gordillo, G. Riboux, and E. S. Quintero. A theory on the spreading of impacting droplets. *Journal of Fluid Mechanics*, 866:298–315, 2019.

[17] K. Range and F. Feuillebois. Influence of surface roughness on liquid drop impact. *J. Colloid Interf. Sci.*, 203:16–30, 1998.

[18] C. Tang, M. Qin, X. Weng, X. Zhang, P. Zhang, J. Li, and Z. Huang. Dynamics of droplet impact on solid surface with different roughness. *International Journal of Multiphase Flow*, 96:56–69, 2017.

[19] M. A. Quetzeri-Santiago, A. A. Castrejón-Pita, and J. R. Castrejón-Pita. The effect of surface roughness on the contact line and splashing dynamics of impacting droplets. *Scientific Reports*, 9(1):1–10, 2019.

[20] I. V. Roisman, A. Lembach, and C. Tropea. Drop splashing induced by target roughness and porosity: The size plays no role. *Advances in Colloid and Interface Science*, 222:615–621, 2015.

[21] L. Xu. Liquid drop splashing on smooth, rough, and textured surfaces. *Phys. Rev. E*, 75:056316, May 2007.

[22] Peichun Tsai, Roeland C. A. van der Veen, Matthias van de Raa, and Detlef Lohse. How micropatterns and air pressure affect splashing on surfaces. *Langmuir*, 26(20):16090–16095, 2010.

[23] A. N. Lembach, H.-B. Tan, I. V. Roisman, T. Gambaryan-Roisman, Y. Zhang, C. Tropea, and A. L. Yarin. Drop impact, spreading, splashing, and penetration into electrospun nanofiber mats. *Langmuir*, 26(12):9516–9523, 2010.

[24] H. Kim, U. Park, C. Lee, H. Kim, M. Hwan Kim, and J. Kim. Drop splashing on a rough surface: How surface morphology affects splashing threshold. *Applied Physics Letters*, 104(16):161608, 2014.

[25] R. de Jong, O. R. Enríquez, and D. van der Meer. Exploring droplet impact near a millimetre-sized hole: comparing a closed pit with an open-ended pore. *Journal of Fluid Mechanics*, 772:427–444, 2015.

[26] A. L. Yarin, I. V. Roisman, and C. Tropea. *Collision Phenomena in Liquids and Solids*. Cambridge University Press, 2017.

[27] H. Almohammadi and A. Amirfazli. Asymmetric spreading of a drop upon impact onto a surface. *Langmuir*, 33(23):5957–5964, 2017.

[28] C. Mundo, M. Sommerfeld, and C. Tropea. Droplet-wall collisions: Experimental studies of the deformation and breakup process. *Int. J. Multiphase Flow*, 21:151–173, 1995.

[29] J. Hao and S. I. Green. Splash threshold of a droplet impacting a moving substrate. *Phys. Fluids*, 29:012103, 2017.

[30] H. Almohammadi and A. Amirfazli. Understanding the drop impact on moving hydrophilic and hydrophobic surfaces. *Soft Matter*, 13:2040–2053, 2017.

[31] S. Buksh, H. Almohammadi, M. Marengo, and A. Amirfazli. Spreading of low-viscous liquids on a stationary and a moving surface. *Exp Fluids*, 60:76, 2019.

[32] Sikalo, C. Tropea, and E.N. Ganic. Impact of droplets onto inclined surfaces. *Journal of Colloid and Interface Science*, 286(2):661 – 669, 2005.

[33] N. Laan, K. G. de Bruin, D. Bartolo, C. Josserand, and D. Bonn. Maximum diameter of impacting liquid droplets. *Phys. Rev. Applied*, 2:044018, Oct 2014.

[34] J. Hao, J. Lu, L. Lee, Z. Wu, G. Hu, and J. M. Floryan. Droplet splashing on an inclined surface. *Phys. Rev. Lett.*, 122:054501, 2019.

[35] S. Lejeune and T. Gilet. Drop impact close to the edge of an inclined substrate: Liquid sheet formation and breakup. *Phys. Rev. Fluids*, 4:053601, 2019.

[36] L. Xu, W. W. Zhang, and S. R. Nagel. Drop splashing on a dry smooth surface. *Phys. Rev. Lett.*, 94:184505, 2005.

[37] G. Riboux and J. M. Gordillo. Experiments of drops impacting a smooth solid surface: A model of the critical impact speed for drop splashing. *Phys. Rev. Lett.*, 113:024507, 2014.

[38] J. M. Gordillo and G. Riboux. A note on the aerodynamic splashing of droplets. *Journal of Fluid Mechanics*, 871:R3, 2019.

[39] C. D. Stow, M. G. Hadfield, and J. M. Ziman. An experimental investigation of fluid flow resulting from the impact of a water drop with an unyielding dry surface. *Proc. R. Soc. Lond.*, 373(A):419–441, 1981.

[40] T. de Goede, K. de Bruin, N. Shahidzadeh, and D. Bonn. Droplet splashing on rough surfaces. *Phys. Rev. Fluids*, 6:043604, 2021.

[41] S. Kim, Z. Wu, E. Esmaili, J. J. Dombroskie, and S. Jung. How a raindrop gets shattered on biological surfaces. *Proceedings of the National Academy of Sciences of the United States of America*, 117(25):13901–13907, 2020.

[42] E. S. Quintero, G. Riboux, and J. M. Gordillo. Splashing of droplets impacting superhydrophobic substrates. *Journal of Fluid Mechanics*, 870:175–188, 2019.

[43] M. A. Quetzeri-Santiago, K. Yokoi, A. A. Castrejón-Pita, and J. R. Castrejón-Pita. Role of the dynamic contact angle on splashing. *Phys. Rev. Lett.*, 122:228001, 2019.

[44] G. Riboux and J. M. Gordillo. Maximum drop radius and critical weber number for splashing in the dynamical leidenfrost regime. *J. Fluid Mech.*, 803:516–527, 2016.

[45] G. Riboux and J. M. Gordillo. The diameters and velocities of the droplets ejected after splashing. *J. Fluid Mech.*, 772:630–648, 2015.